NASA CR 134623
UM 026030-5-F

Final Report

TWO PHASE DETONATION STUDIES

by

J. A. NICHOLLS
T. H. PIERCE
H. MIYAJIMA
R. OZA
P. PATIL

THE UNIVERSITY OF MICHIGAN
Department of Aerospace Engineering
Ann Arbor, Michigan 48105

prepared for

NATIONAL AERONAUTICS AND SPACE ADMINISTRATION

May 1974

Grant NGL 23-005-336

NASA Lewis Research Center
Cleveland, Ohio
R. J. Priem, Project Manager

NASA CR 134623
UM 026030-5-F

Final Report

TWO PHASE DETONATION STUDIES

by

J. A. Nicholls
T. H. Pierce
H. Miyajima
R. Oza
P. Patil

The University of Michigan
Department of Aerospace Engineering
Ann Arbor, Michigan 48105

prepared for
National Aeronautics and Space Administration

May 1974

Grant NGL 23-005-336

NASA Lewis Research Center
Cleveland, Ohio

R. J. Priem, Project Manager

1. Report No.	2. Government Accession No.	3. Recipient's Catalog No.
NASA CR 134623		

4. Title and Subtitle	5. Report Date
Two Phase Detonation Studies	May 1974
	6. Performing Organization Code

7. Author(s)	8. Performing Organization Report No.
J.A. Nicholls, T.H. Pierce, H. Miyajima, R. Oza, P. Patil	UM 026030-5-F
	10. Work Unit No.

9. Performing Organization Name and Address	11. Contract or Grant No.
The University of Michigan Department of Aerospace Engineering Gas Dynamics Laboratories Ann Arbor, Michigan 48105	NGL 23-005-336
	13. Type of Report and Period Covered
12. Sponsoring Agency Name and Address	Contractors Report 2/1/73-2/1/74
National Aeronautics and Space Administration Washington, D.C. 20546	14. Sponsoring Agency Code

15. Supplementary Notes

Project Manager, Richard J. Priem, Chemical Propulsion Division, NASA Lewis Research Center, Cleveland, Ohio

16. Abstract

This report describes the research conducted in the past year of this grant. An experimental study of the passage of a shock wave over a burning fuel drop is described. This includes high speed framing photographs of the interaction taken at 500,000 frames per second. A theoretical prediction of the ignition of a fuel drop by a shock wave is presented and the results compared with earlier experimental work. Experimental attempts to generate a detonation in a liquid fuel drop (kerosene) — liquid oxidizer drop (hydrogen peroxide) — inert gas — environment are described. In this connection an appendix is included which gives the analytical prediction of power requirements for the drop generator to produce certain size drops at a certain mass rate. A Bibliography is also included which lists all of the publications resulting from this research grant.

17. Key Words (Suggested by Author(s))	18. Distribution Statement
Detonation Shock Waves Droplet Combustion	Unclassified - unlimited

19. Security Classif. (of this report)	20. Security Classif. (of this page)	21. No. of Pages	22. Price*
Unclassified	Unclassified	101	

* For sale by the National Technical Information Service, Springfield, Virginia 22151

FOREWORD

This represents the final report on NASA Grant NGL 23-005-336. For the most part, the report presents the progress made in the calendar year of 1973, although some earlier work is included where needed for completeness or continuity. No attempt is made to repeat research findings that are already adequately documented in the literature.

The study was under the direction of Professor J.A. Nicholls, Department of Aerospace Engineering. Dr. R.J. Priem, NASA Lewis Research Center, was program manager.

TABLE OF CONTENTS

LIST OF FIGURES

LIST OF TABLES

ABSTRACT

This report describes the research conducted in the past year of this grant. An experimental study of the passage of a shock wave over a burning fuel drop is described. This includes high speed framing photographs of the interaction taken at 500,000 frames per second. A theoretical prediction of the ignition of a fuel drop by a shock wave is presented and the results compared with earlier experimental work. Experimental attempts to generate a detonation in a liquid fuel drop (kerosene)—liquid oxidizer drop (hydrogen peroxide)—inert gas—environment are described. In this connection an appendix is included which gives the analytical prediction of power requirements for the drop generator to produce certain size drops at a certain mass rate. A Bibliography is also included which lists all of the publications resulting from this research grant.

I. INTRODUCTION

This final report comes at the end of a number of years research on the subject of heterogeneous detonations. The motivation for this work stemmed from liquid propellant rocket motor combustion instability, although certainly the results are also applicable to other jet propulsion engines, internal combustion engines, safety aspects of spilled liquid fuel, coal mine explosions, airplane crashes, fuel air explosions, etc. The research program had been divided into phases and sub-phases, many of which had terminated earlier. The topics considered here include the passage of a shock wave over a drop which is already burning, a theoretical treatment of the ignition of a drop by a shock wave, and the experimental attempt to generate a detonation in a liquid fuel drop—liquid oxidizer drop—inert gas mixture. Also an appendix is included which presents the theoretical prediction of the power requirements for generating liquid drops of a given size and amount. A Bibliography is also included which lists all of the publications resulting from this research grant.

II. RESEARCH RESULTS

PHASE A. PASSAGE OF A SHOCK WAVE OVER A BURNING DROP

In rocket motors and other combustion devices, fuel drops are often burning when disturbed by a pressure and velocity perturbation. In such cases the process of combustion of the drop may be terminated or altered as to rate of combustion. Of course, this alters the combustion stability characteristics of the motor. In an effort to study this problem an experimental technique has been developed which allows a single burning fuel drop to fall free in the horizontal test section of a shock tube. A controlled pressure and velocity pulse is then passed over the drop in the form of a shock wave. The ensuing interaction process is then examined through use of image converter camera photography, luminosity measurements, and (in the past year) ultra high speed schlieren framing camera photography. The particular types of interaction studied include the cases of a non-ignited drop, the pre-ignited drop which is extinguished by the shock, the pre-ignited drop which continues to burn with a wake flame, and the ignition of a non-burning drop by the shock wave. The results obtained served to show the qualitative nature of the interaction, the deformation of the drops, the acceleration of the drops, the break-up time, and the threshold conditions between blow-off and the wake flame conditions.

A description of the experimental technique and the earlier results obtained are given elsewhere[1, 2, 3]. However, some of this will be repeated

here for the sake of completeness and continuity. The high speed photographic study is presented for the first time and includes some improvements in the experimental technique.

1. Experimental Apparatus and Procedure

A horizontal shock tube consisting of a driver section, driven section, dump tank, and diaphragm section was used for these studies. The driver section was 3 in. I. D. and 5 ft long which allowed for a sufficient duration of uniform convective flow behind the incident shock. The driven section was 12 ft long with a rectangular cross section of 1. 5 in. x 2. 5 in. The test section was located 9 ft from the end of the diaphragm section with schlieren quality plate glass windows 11 3/4 in. long and 1 in. wide. The shock tube was fired by venting the gas between the two diaphragms of the diaphragm section.

The procedure for obtaining a time history of deformation and disintegration of a drop was either taking a series of spark shadow photographs at different time intervals after the shock wave intercepted the drop or taking a streak photograph through a 1/8 in. wide horizontal slit. Every spark photograph taken by the first method was that of a different drop. The run to run reproducibility of the drops was not very good due to the drop injection system used but the essential features of the time history of the interaction were retained. Spark photographs were taken with a Beckman and Whitley Model 501A image converter camera at the exposure time of

1.0 microsecond. Appropriate timing was obtained by the built-in time delay unit of a Tektronix Type 565 dual beam oscilloscope which was triggered by the incident shock wave passing over a pressure switch flush mounted on the wall of the shock tube upstream. A modified Beckman and Whitley Dynafax rotating drum camera was employed for obtaining streak pictures.

The shock speed was determined by the measured time interval for the shock wave to travel 2 ft between a pressure switch and a Kistler pressure transducer. A pressure switch was used for triggering the counting because of its insensitivity to the noise produced by the electric spark for the fuel drop ignition.

For the test of flame blow-off, an RCA 929 photomultiplier tube and a Texas Instrument LS 400 phototransistor were used.

The method for producing a suspended ignited drop in the test section was based on the sudden retraction of a hypodermic needle from which the drop was suspended. The electrode, which produced the ignition spark shortly before retraction, was assembled to the needle system and retracted with the needle. The needle-electrode assembly is shown in Fig. 1.and the needle tip configuration in Fig. 2. A synchronizing signal from the firing of the shock tube activated the ignition spark as well as the solenoid which withdrew the locking pin and allowed the needle assembly to retract rapidly. Synchronization was accomplished either by the shock wave

passing over the pressure switch 8.05 ft upstream of the drop injection position or by the breakage of a thin copper wire on the diaphragm of the high pressure section. The method used depended on the test shock Mach number. The drop injection system was covered by a dome to facilitate evacuation and filling of the shock tube.

The more recent high speed framing photography study involved some changes from the foregoing. In the earlier studies the single drop produced often had a tail (thus resembling a tadpole) or the spark discharge tended to distort or shatter the drop. Consequently a number of changes were made to the drop suspension capillary and electrode. For one thing, the piano wire (shown in Fig. 2) was extended beyond the exit of the suspension capillary. This allowed the drop to be suspended by the wire with a consequent marked reduction in wetted area and, hence, deformation to the drop when retraction occurred. Also the negative electrode was extended to the surface of the drop, thus reducing deformation due to spark discharge. A thin mylar shield, painted black, was introduced to shield light emitted by the spark from the transient light detector. The insulating material used for the positive electrode was replaced by teflon to prevent high voltage breakdown. The solid wire used to connect the drop suspension capillary and the retraction springs was replaced by a stranded steel wire. This improvement virtually eliminated frequent failures of the wire. Finally, the fuel was introduced to the capillary

by gravity feed rather than by pressurizing the fuel tank. The net result of all of these changes was to produce a good single spherical drop, reproducible in size from run to run.

Experiments involving the use of higher Mach number shocks encountered difficulty in synchronizing the firing of the shock tube with injection of the fuel drop. It was found that at the higher Mach numbers the shock arrived in the test section before the needle was completely retracted, thus resulting in damage to the needle and electrodes. Consequently a new technique was developed which uses an exploding wire sandwiched between two mylar diaphragms. Energy stored in a capacitor (100 joules) is used to explode the wire with consequent rapid diaphragm rupture. The sequence of events, then, is as follows. The drop was suspended and ignited by a spark at a suitable point in the test section and was allowed to fall freely from the capillary. The light emitted by the falling-burning-drop was detected by a transient light detector which, in turn, fired the capillary retraction unit and the retraction monitor circuit (see Fig. 3). The retraction monitor signal was used to activate a delay unit to generate the high energy pulse to rupture the mylar diaphragms. A signal from a pressure switch (upstream of the test section) was used to trigger the oscilloscope and delayed output from the scope was used to trigger a pulse light output from the xenon lamp.

For the high speed photographic study a Beckman-Whitley 330 framing camera was used at a speed of 480,000 frames/sec for an approximate duration of 160 μsec in order to record the interaction of the shock with the drop. Schlieren optics were employed. Of course, this allowed the complete interaction to be obtained in one run, whereas with the earlier image camera records only one photograph per run could be made.

For the experiments, the test section gas was either oxygen, nitrogen, or air, with various initial pressure levels, P_1, possible. Various shock Mach numbers, M_s, were generated. The fuel used was diethylcyclohexane (DECH).

2. Results and Discussion

Image converter camera photographs of the interaction of an $M_s = 2.02$ shock with a 1.6 mm DECH drop in one atmosphere of O_2 are shown in Fig. 4. A weak bow shock can be seen in some of the photographs. Disturbances from secondary drops, or the "tail" of the parent drop when the needle is suddenly retracted, are to be noted in some cases. It is noted that the incident shock wave is accelerated in the hot region (see Run Nos. 31, 20 and 55). The initial flame appears to be laminar but becomes turbulent as it is blown off the parent drop and into the wake by the convective flow behind the shock wave. The initial flame apparently ignites the cloud of smaller drops shed from the parent drop (micromist)(see Run No. 55). The flame attached to the wake of the

disintegrating drop (wake flame) becomes fully developed when the rate of micromist shedding attains some level, as is seen in Run Nos. 53 and 25. The parent drop apparently acts as a flame holder. At the later stages of interaction, the bow shock is reflected from the bottom and the top of the shock tube walls as is seen in the pictures of Run Nos. 24, 25, and 53. Comparison of these results with similar ones for non-ignited drops shows that the lateral deformation of drops is larger in initially ignited drops than non-ignited ones, and that the micromist shed from the drops which have a wake flame is consumed much faster than that from non-ignited drops.

Under certain conditions of drop size, shock Mach number, and initial pressure, the flame will not stabilize in the wake but will be blown off. In those cases the disintegrating drop rapidly takes on the appearance of the non-ignited drop.

Streak photographs show a continuous recording of the interaction of a shock with one drop. Figures 5 and 6 are streak schlieren photographs of non-ignited and ignited drops in pure oxygen with an initial pressure of 30 in. Hg. The shock Mach number is about 1.7 so that the flow behind the shock wave is subsonic and hence compression waves are seen to be transmitted upstream. Comparison of Figs. 5 and 6 shows an apparent effect of the wake flame on break-up characteristics. The curvature of the trajectory of the drop at the leading edge changes

abruptly at about the end of the break-up on the streak photograph or on the x-t plane. The break-up time of a drop, t_b, which is defined as the time from the instant when the incident shock intercepts the drop until the disintegrating drop is accelerated to 60% of the convective flow velocity behind the incident shock wave seems to be longer in the case of a drop which has a wake flame. The opaqueness of the wake in Fig. 5 is attributable to the microspray droplets whereas in Fig. 6 these drops have vaporized and burned.

Figure 7 shows the deformation of drops (i. e., the ratio of the maximum width of dense area d perpendicular to the flow to the initial diameter d_0) with time elapsed from shock passage through the center of the drop. Data is shown for drops with a wake flame as well as for non-ignited drops. The solid lines in the figure are the correlation of Ranger and Nicholls[5] for water drops. The deformation of the non-ignited drops are in good agreement with this correlation but, as noted, the drops with a wake flame produce much larger deformations. Similar data obtained for the "blow-off" case indicated somewhat greater deformation than for the non-ignited case but not as large as that of the drops with a wake flame. The surface tension of DECH is 28 dynes/cm, while that of water is 73 dynes/cm at 20°C. In view of the fact that the DECH deformation is correlated well with the equation derived from experiment with water, the effect of surface tension may not be large. Also, the viscosities of

DECH and water are about the same. Hence, it is tentatively concluded that the differences in deformation are largely attributable to altered pressure distributions around the drop as a consequence of the flame.

In spite of the fact that the original drop is changing shape and losing mass by micromist shedding, it is interesting to consider the drop as a spherical particle of constant mass. Then the displacement of the drop can be expressed as

$$\frac{x}{d_o} = K\left[\frac{U_2}{d_o}\sqrt{\frac{\rho_2}{\rho_\ell}}\,t\right]^2 \qquad (1)$$

or,

$$\bar{x} = \bar{K}\bar{T}^2$$

where, $\bar{x}$ = dimensionless distance

$\bar{T}$ = dimensionless time

$K = 3/8\ C_{D_0}$, and C_{D_0} is the apparent drag coefficient based on the initial diameter of the drop, x is the displacement of the leading edge of the drop along the flow from the original position, U_2 and ρ_2 are the velocity and density behind the incident shock, respectively, d_o is the original drop diameter, ρ_ℓ is the density of the liquid drop, and t is the time after the beginning of interaction. Constant acceleration is assumed and relative velocity between gas and drop, drag coefficient, and drop diameter are evaluated at $t = 0$.

The displacement of the drop satisfies Eq. (1) under all the test conditions reported here for a good fraction of the break-up time. Figure 8 is an example. The apparent drag coefficient was determined from such displacement data and indicated little variation with Reynolds number. The Mach number of the convective flow did vary some in various runs but this effect was not isolated. The averaged values of C_{D_0} are: 1. 80 for drops with a wake flame, 2. 10 for non-ignited drops, and 2. 66 for drops with "blown off" flames. The drag coefficient for the drops with a wake flame is the smallest, probably due to the altered pressure distribution.

Drop break-up time, t_b, was found to be somewhat larger for drops with a wake flame.

For the determination of "blow off" limit, two types of photoelectric sensors were used. An RCA 929 photomultiplier tube viewed the whole window of the test section and a Texas Instrument LS 400 phototransistor viewed a small portion at the original drop position. It was easy to conclude from the voltage time outputs of these sensors whether a wake flame or blow-off was realized.

Figure 9 shows the line of demarcation between the wake flame and blow-off regions in the initial pressure—shock Mach number plane. The limiting initial pressure increases at about $M_2 \sim 2$, where the convective flow behind the incident shock is sonic. Otherwise, the limiting initial

pressure is fairly insensitive to the Mach number. Other experiments, conducted with a 75% O_2-25% N_2 mixture, yielded very similar behavior but with higher limiting initial pressure values.

The high speed framing camera results will now be discussed. The various cases studied are indicated in Table I.

Table I. Test Conditions, High Speed Photography

Case	Initial Condition	Test Section Medium	Mach No.	Pressure In./Hg	After Interaction	Drop Size μm (approx.)
a.	Non-ignited	Nitrogen	2.05	29.1	Non-ignited	1500
b.	Ignited	Air	2.05	29.1	Extinguished	1250
c.	Ignited	Oxygen	2.05	29.1	Burning	1250
d.	Non-ignited	Nitrogen	3.5	11.5	Non-ignited	1500
e.	Non-ignited	Oxygen	3.5	11.5	Ignited	1500

Photographic sequences of these various cases were obtained.

Figure 10 shows the comparison between cases a, b, and c, each of them taken at the same time after interacting with the shock ('0' micro-seconds corresponds to the instant when the shock hits the parent drop). In these photographs there is, for the most part, only one drop. However, the window quality is not good and there are smudges and vertical marker lines on the windows. The pre-ignited drop is injected approximately

1/2 in. above the center line of the test section and burns for about 100 milliseconds before interaction with the shock. This is the reason for the presence of column of hot gases in the cases b and c. When the incident shock enters the region of hot gases surrounding the drop, depending on the acoustic impedance of the cold uniform region and the hot gases in the flame, transmitted and reflected waves will be obtained at the interface. Hence, it is plausible to expect a significant difference between the wake structures in the cases a, b, and c, as can be seen in Fig. 10. The upward shift in the wake of the drop is not because of buoyancy effect (since Grashoff number $\ll$ 1) but due to the altered shock structure and shape when it enters the hot region. The combustion products generated before shock arrival are seen to blow downstream. In case b the flame is blown-off and no further combustion occurs; the subsequent drop breakup process then resembles case a. In case c combustion continues in the wake of the drop.

The structure of the wake is considerably affected by the drop breakup characteristics and also by the extent of micromist evaporation. In the case of the wake burning in oxygen, the micromist evaporation process will be enhanced due to higher flame temperature and thus micromist will contribute to the mass of gaseous contents of the recirculation, thereby reducing the mass entrained from the external convective flow. This seems to be the reason for a relatively longer and wider wake

structure in case c. The resultant shallower wake angle can be expected to affect the pressure distribution in the wake considerably because of its effect on the deflection of the external convective flow. In turn, pressure distribution can affect drop acceleration and drop breakup characteristics.

Cases d and e are shown in Fig. 11 wherein neither drop was burning initially. The strong shock was sufficient to ignite the drop when in O_2, case e. Ignition was determined by an appreciable photocell output. In the photographs, ignition is not obvious. However, it must have occurred somewhat before 80 μs in that the length of the visible wake is much less in the last photograph and the shape of the bow shock has been changed. There is some indication of a blast wave interacting with the bow shock in this photograph. Photographs taken at later times indicate the much faster consumption of the drop in the burning case than in the N_2 case.

The differences in the breakup pattern for non-burning drops for the two Mach numbers can be noted by comparing Figs. 10 and 11 for the cases a and d. In both cases it is possible to see the formation of surface waves.

PHASE B. ENERGY RELEASE PATTERNS

1. Theory of Shock Ignition of Fuel Drops

A. Introduction

The essential nature of two-phase detonations is ultimately connected with the manner in which the liquid phase reactant is converted to its vapor phase, and to how the two vapor phase reactants then mix and ignite. In the case of two-phase detonations in which the liquid phase reactant is initially in the form of a spray (of fuel droplets, say), the conversion process involved is that of the interaction of the shock wave with each of the drops individually in the spray. Much empirical data have been gathered which have shown the major characteristics of this particular process for the case of shock interaction with non-reacting drops[4-8]. Unfortunately, must less information is available for the case of reacting drops, which forms the subject of interest here[9-11,14].

Both non-reacting and reacting drops share certain features of a shock-wave interaction. As the shock wave is passing over the initially stationary droplet, very little of consequence occurs. In particular, the drop does not change its velocity during this period while the surrounding gas is accelerated. This produces a flow field around the droplet. If the shock strength is sufficient, the free stream velocity can be supersonic with respect to the drop. Under these circumstances, a bow shock, wake shock, and other characteristics of supersonic flow over a sphere[12] are apparent (Fig. 12).

The drop subsequently contracts along an axis which is parallel to the free stream, and expands in the transverse direction, so that the frontal area exposed to the flow increases with time. The drop also begins to accelerate in the direction of the moving shock.

The fluid near the surface in the drop is set in motion by the boundary layer gases of the convective flow. The liquid boundary layer separates from the droplet and is apparently broken up into a spray of droplets whose diameter is of the order of the boundary layer thickness. This "microspray" (μspray) is thereby introduced into the near wake region of the parent droplet. It appears that, at the same time, a Taylor instability occurs on the front surface of the parent drop, producing waves whose amplitudes grow and will eventually cause "catastrophic" disintegration of the parent drop[13].

After a certain period of time following passage of the incident shock, the parent drop ceases its transverse growth; the frontal diameter thereafter decreases. Whether or not catastrophic breakup due to Taylor instabilities has occurred by this point is not clear. Nonetheless, if the parent drop is reactive, it is somewhat after this time that the ignition of evaporated μspray occurs in the near wake region. The ignition is explosive in character, producing a blast wave.

Beyond this ignition, the process of mass stripping from the parent drop (or its fragments in the event of catastrophic breakup) continues until nothing remains of it. If ignition has occurred, in the reactive case, the

continued stripping supplies fresh fuel to the wake region where it is then consumed. This post-ignition combustion process is usually relatively "smooth"; occasionally, however, multiple explosive ignitions occur in sequence.

Only incident shocks of sufficient strength produce explosive ignition. As a rule, $M_s > 3$ is required, typically. In what follows, it will therefore be assumed that the incident shock is of this strength, and also that the resulting flow field around the parent droplet is initially supersonic.

The capacity to describe the sequence of events, which was qualitatively outlined above, in sufficient detail as to allow reasonable prediction of the time between incident shock contact with a reactive drop and its explosive wake ignition, is of obvious interest. Kauffman[14] suggested a model in which groups of stripped μspray, which move rearward into the wake region, remain as they move in volume elements of fixed identity and fixed geometry. The μspray in each such volume element evaporates, and the vapor produced mixes homogeneously throughout the element. Ignition is identified with that element in which the concentration of fuel is largest; ignition <u>times</u> are assessed from the interval separating incident shock contact and the formation of this element.

Pierce[15] treated a simple model in which stripped μspray enters the wake and therein evaporates and reacts with the hot oxidizer. The energy thus liberated is conducted away to the external flow until the total evaporation rate (which controls the reaction rate) becomes so large that thermal

energy begins to accumulate in the wake region. The point in time at which this occurs is described to be the instant of ignition, since as the temperature of the region increases, the processes responsible for further energy liberation are accelerated.

Recently, Fishburn[13,16] has suggested that the density of μspray drops (in the wake region of the parent drop) during the first period following incident shock passage, produces local fuel vapor concentrations which are too low to support explosive ignition. That is, boundary layer stripping of the contiguous parent droplet is considered to be too slow a process to allow for high μspray densities. Therefore it is argued that fragmentation of the parent drop, through Taylor instabilities, must first occur; each fragment then individually strips, resulting in a much higher rate of μspray production. Again, the μspray drops enter the wake, evaporate and react, and a chemical induction time is added (to the time until fragmentation occurs) to obtain the overall ignition delay.

Each of these theories shows some degree of agreement with the available experimental ignition time data[9,11,14], yet none, in itself, is able to convincingly explain all of the observations made of the ignition process. The ability to extend any one of these computations to reliably include a wide range of fuel/oxidizer combinations is rather questionable. It is the purpose of the present exploratory study to contribute towards the development of a unified theory of shock induced reactive droplet ignition.

B. Theoretical Model

In its present form the sequence of events leading to explosive ignition is considered as comprised of two separate intervals; namely, a "dormant" period, followed by an "active" period. As such, this model is similar in kind to Fishburn's two-stage model. That is, if the same terminology were applied to that model, the "dormant" and "active" periods would correspond to the intervals before and after parent drop fragmentation, respectively. It is to be emphasized at the outset that the two periods in the following formulation both differ qualitatively (as well as quantitatively) from the Fishburn model.

(i) Dormant Period

This period begins upon initial contact by the incident shock with the spherical parent droplet in its undisturbed, motionless state. Four processes are initiated. First, the droplet begins to accelerate. This in turn initiates the development of Taylor instabilities on the forward surface. At the same time, the droplet begins to flatten, and the boundary layer formation in the liquid surface commences.

Complete boundary layer formation requires a nontrivial induction time[17], however, it is believed that the mass stripping process begins well before the liquid boundary layer is fully developed. This is based on the many early-time photographs such as in Fig. 13, as well as on mass loss measurements[6]. In any event, it is clear that the mass loss rate accelerates with increasing time during this period. In fact, Reinecke[6] has obtained

a reasonable empirical correlation for mass loss, assessed from x-ray photographs of stripping water drops, which is

$$\frac{m}{m_o} = \frac{1}{2}\left[1 + \cos \pi (t/t_s)\right] \quad . \tag{1}$$

The mass, m, of the droplet at any time, t, during the breakup process is thus correlated with its initial mass, m_o, and the time to complete disintegration, t_s (stripping time).

As the droplet continues to flatten, its frontal diameter increases rapidly. Fluid in the liquid boundary layer, which travels from the forward stagnation point to the maximum perimeter before separating into μspray, thus travels progressively further before being stripped off. This, as well as the fact that the boundary layer becomes more fully developed with passing time, leads to the expectation of increased μspray size with increasing time.

No widely accepted means of computing μspray sizes and separation velocities exists. There is some agreement, however, that the μspray diameter should be of the order of the liquid boundary layer thickness just prior to its separation[14, 15]. Most analytical estimates predict μspray diameters of the order of .01 of the parent drop diameter, which roughly agrees with what experimental evidence is available[4, 7].

For example, the separation process can be envisioned to proceed in two stages: First, an annular sheet or film of fluid is shed from the drop

periphery, and second, this sheet breaks up into the μspray drops by means of a process similar to that which occurs in the breakup of a free liquid jet[18]. The micromist drops can, by that analogy, be expected to have diameters which are approximately twice the thickness of the sheet. The sheet thickness itself is estimated by imposing conservation of mass and momentum on the fluid which enters it, between the positions just before separation (when the fluid is in the parent drop boundary layer) and just after separation (when the fluid is in the annular sheet and has a flat velocity profile).

When the liquid boundary layer is assumed to have a Taylor velocity profile[5], this particular means of analysis produces reasonable early-time mass loss rates and μspray sizes[15]. In addition, the velocity of the μspray when it separates from the parent drop, u_d, can be readily derived to the form

$$\frac{u_d}{u_c} = \frac{A}{\sqrt{2}} \quad . \tag{2}$$

In which u_c is the relative convective flow velocity, while

$$A = \left(\frac{\rho_2 \mu_2}{\rho_\ell \mu_\ell} \right)^{1/3} \tag{3}$$

and ρ_ℓ, μ_ℓ, ρ_2, μ_2 are the densities and viscosities of the liquid and of the free stream convective flow.

It is reasonably clear that boundary layer stripping cannot account for the mass loss rates over the entire breakup time. The surface wave concept of Collins[19] or the Taylor instability theory of Fishburn[13] is needed at later times to explain the high stripping rates. It is believed, however, that simple boundary layer stripping predominates the early stages of breakup, and Eq. (2), in spite of its crudeness, serves to show that $u_d/u_c = O(10^{-1})$ for typical intermediate shock strengths and typical fuel/oxidizer combinations. That is, the fluid separates from the parent drop at velocities which are always much lower than the prevailing free stream gas velocity.

The velocity at which the point of separation moves in the transverse (or, radial) direction due to drop flattening may be evaluated from the well accepted empirical form[20]

$$\overline{D} = 1 + \alpha \overline{T} \tag{4}$$

in which $\overline{D}$ is the ratio of parent drop frontal diameter at time t to its initial (undisturbed) diameter, D_o, and

$$\overline{T} = \frac{u_2}{d_o} \beta^{1/2} t \tag{5}$$

is the non-dimensional time, $\beta = \rho_2/\rho_\ell$, u_2 is the free stream gas velocity relative to the drop at $t = 0$, and α is a correlating coefficient whose value is $\alpha \simeq 1.70$. From Eq. (4), the radial velocity, u_r, of the separation point is

$$u_r/u_c = (1/2)\,\alpha\beta^{1/2}\,(u_2/u_c) \quad . \tag{6}$$

The radial velocities computed from Eq. (6) show that u_r/u_c is also $O(10^{-1})$.

The inference from these two simple results is that in general the separated liquid film can be expected to turn in the direction of the prevailing local flow field while it is still contiguous with the parent drop (i.e. before breaking up into μspray drops). When the external flow field is subsonic, the μspray is in this fashion carried rearward, more or less parallel to the axis of symmetry. It is gradually accelerated, and ultimately reaches the convective flow velocity. An example of this is shown in Fig. 14.

When the flow field is supersonic, which is the case of interest here, it appears that the separated film is turned inward by the flow structure, in such a way that the μspray is initially carried into the free shear layer of the near wake, above the recirculation zone. It subsequently becomes engulfed in the expanding recirculation zone itself, and most does not escape, having entered at low velocity. This results in a remarkably well-defined recirculation zone, as in Figs. 15 and 16.

In fact, the rearward velocity of the recirculation zone tip can be estimated by noting that its geometry remains roughly constant while the parent drop is growing. Since the droplet growth rate is given by Eq. (6), the rate of growth in recirculation zone length is simply

$$dL/dt = u_r \text{ ctn } \beta \tag{7}$$

in which β is the recirculation zone angle with respect to the axis. For typical supersonic wakes, $4 < \text{ctn } \beta < 6$. Equation (7) then shows that $dL/dt \ll u_2$, even for the larger value of ctn β. The actual velocity of the recirculation zone tip, measured from streak photographs such as Fig. 15(b), agrees with the order of magnitude predicted by Eq. (7). (It should be observed that the recirculation zone is not filled by microspray in the subsonic case and so it is not visible on photographs such as Fig. 14.

Within the recirculation zone, the trapped μspray move with the low velocity vortices and evaporate. If a given μspray drop is formed at time τ (measured after incident shock contact with the parent drop), with initial diameter $d_{M_o}(\tau)$, then its diameter at time t (i. e. after an interval t-τ) can be approximated by the quiescent evaporation rate expression[21]

$$d_M(t,\tau) = \begin{cases} \left[d_{M_o}^2(\tau) - 2C\,(t-\tau)\right]^{1/2}, & t \leq t_{ex} \\ 0 & t \geq t_{ex} \end{cases} \tag{8}$$

in which

$$C = \frac{4k}{C_p \rho_\ell} \ln\left[1 + \frac{C_p}{\mathcal{L}}(T_g - T_\ell)\right], \tag{9}$$

where k is the coefficient of thermal conductivity of the gas, T_g is its temperature, and C_p its specific heat, and $\mathcal{L}$ and T_ℓ are the latent heat and temperature of the liquid μspray drop. The time to extinction of the μspray drop (complete evaporation), t_{ex}, is

$$t_{ex} - \tau = \frac{d_{M_o}^2(\tau)}{2C} \quad . \tag{10}$$

The rate of mass evaporation from this μspray drop at time t is

$$\overline{\dot{m}}_{ev}(t,\tau) = C_2\, d_M(t,\tau) \quad , \tag{11}$$

where $C_2 = \pi \rho_\ell\, C/2$.

These formulae allow computation of the total amount of fuel vapor which has evaporated from all μspray drops in the recirculation zone up to time t, taking into account the time varying initial μspray size, in the following manner. First, the number of μspray drops, δn, which are formed during an interval, $\delta\tau$, about time τ, is

$$\delta n(\tau) = \frac{\dot{m}(\tau)\ \delta\tau}{m_{M_o}(\tau)} \tag{12}$$

where $\dot{m}(\tau)$ is the parent drop stripping rate, at $t = \tau$, and $m_{M_o}(\tau)$ is the mass of the μspray drops formed at that time; i. e. $m_{M_o}(\tau) = \rho_\ell\, \pi\, d_{M_o}^3(\tau)/6$. The contribution at time $t > \tau$ to the total μspray evaporation <u>rate</u> from μspray drops formed at $t = \tau$ is

$$\delta\dot{m}_{ev}(t) = \overline{\dot{m}}_{ev}(t,\tau)\ \delta n(\tau)$$

or, in the limit,

$$d\dot{m}_{ev}(t) = C_2\, d_M(t,\tau)\, \frac{\dot{m}(\tau)}{m_{M_o}(\tau)}\, d\tau \quad . \tag{13}$$

Therefore, the total evaporation rate, at time t, due to all μspray drops present in the recirculation zone at that time, is found by integrating Eq. (18) over all $\tau \leq t$; namely,

$$\dot{m}_{ev}(t) = C_2 \int_{\tau=0}^{t} \frac{\dot{m}(\tau)\ d_M(t,\tau)}{m_{M_o}(\tau)}\, d\tau \quad , \tag{14}$$

and the total mass of fuel vapor evaporated from all μspray drops prior to time t is

$$m_{ev}(t) = C_2 \int_{t^*=0}^{t} \int_{\tau=0}^{t^*} \frac{\dot{m}(\tau)\ d_M(t^*,\tau)}{m_{M_o}(\tau)}\, d\tau\, dt^* \quad . \tag{15}$$

A simple parent drop stripping rate which can be used is

$$\dot{m}(\tau) = \frac{\pi m_o}{2t_s} \sin \frac{\pi\tau}{t_s} \quad , \tag{16}$$

which derives from Eq. (1), by differentiation, and the time varying μspray size, $d_{M_o}(\tau)$ is obtained in the fashion described earlier. Then, upon appropriate selection of values for the parameters which appear in Eq. (9), the vapor accumulation in the recirculation zone, m_{ev}, can be computed from Eq. (15) as a function of time.

It is noted parenthetically that m_{M_o} is, of course, never actually zero, but that, on the other hand, $\dot{m}(\tau)$ is zero at $\tau = 0$. That is, actual parent drop stripping can begin only when the liquid boundary layer has developed

to the point that its kinetic energy cannot be dissipated by the liquid surface at the point of separation. This occurs, approximately, when the balance

$$2\sigma_\ell \pi D = (1/2)\ \rho_\ell \pi D \int_0^{d_s} u_\ell^2\ (y, t)\ dy \qquad (17)$$

occurs, in which σ_ℓ is the liquid surface tension, $u_\ell(y, t)$ is the time-varying liquid boundary layer velocity profile (measured inward from the surface at the point of separation), D is the parent drop frontal diameter, and d_s is the thickness of the annular sheet, when it is separated. This concept of a "boundary layer induction time" is indeed similar in spirit to that of Ranger[5], but it does not require that the boundary layer be fully established before initiation of stripping. For the present purposes, an estimate of the minimum film thickness, from Eq. (17), was used to compute $m_{M_o}(0)$ required in Eq. (15).

Characteristic calculations from Eq. (15) are summarized in Figs. 17 and 18, for the case of diethylcyclohexane (DECH) drops in oxygen. The vapor accumulation, at the moment, t*, of maximum droplet expansion, is shown in Fig. 17 as a fraction of the total mass removed from the parent drop up to that time, m_{st}. Figure 18 shows the maximum μspray initial diameter, $d_{M_o}(t^*)$. The effect of initial pressure, P_1, as well as parent drop initial diameter, D_o, and incident shock Mach number, M_s is

demonstrated. The extent of the evaporation which has occurred by t* is surprisingly small for D_o somewhat larger than 300μ.

The equivalence ratio, ϕ, corresponding to the accumulation of fuel vapor within the recirculation zone at t*, is shown on Fig. 19. Equivalence ratio is defined as the quotient of actual fuel/oxidizer ratio to the stoichiometric fuel/oxidizer ratio, so that $\phi = 1$ represents the stoichiometric condition. It is observed that at reduced pressures and for small parent drop sizes, the equivalence ratio could reach significant values. The calculations indicate, however, that the accumulation rates are slow; i. e. $\dot{m}_{ev}(t)$ from Eq. (14) is never very large for parent drops which are larger than 300μ diameter.

From these results, three conclusions can be drawn. First, the recirculation zone does not impulsively reach an extremely fuel rich condition (as was initially suspected). On the contrary, the region is generally quite lean; second, in those cases for which m_{ev} is non-negligible, continuous reaction with the hot oxidizer will preclude accumulation of fuel vapor to the extent indicated in Fig. 19. Moreover, at time t*, most of the liquid fuel which was stripped from the parent drop resides in its recirculation zone in the form of unevaporated μspray. Therefore, there is little possibility that the recirculation zone can itself support an explosive ignition. In fact, when ignition occurs, the entire wake region is consumed except for the recirculation zone, as can be seen in Fig. 20.

(ii) Active Period

The frontal diameter of the parent drop reaches its maximum when $t = t^*$; t^* correlates roughly with $\overline{T} = 1.3$. Catastrophic breakup, as predicted by Fishburn[13], would have occurred prior to this time; viz., approximately at $\overline{T} = 0.9$. It is not completely clear as to whether or not this is in fact the case, and, in any event, the aggregate representing the remaining parent drop shows no abrupt change in velocity during this period. If it has been shattered into fragments, these fragments, as a closely packed group, evidently, thereafter, behave as a single (porous) body. Fragmentation would, of course, explain the accelerated stripping rates (which occur at about this time), but Collins' surface wave theory[19] does so equally well. The experimental data available at this writing simply do not allow for discrimination between these two possibilities.

Nevertheless, it is not essential to the present phenomenological description of ignition that the cause for accelerated mass removal be actually identified, because a change in the stripping mechanism does not appear to be the single event that is primarily responsible for eventual explosive ignition. Instead, it appears that the termination of parent drop flattening, which allows the escape of substantial quantities of μspray from the near wake region, is responsible for the final events leading to ignition. That is, μspray which is shed during the period following time t^* is not engulfed by an expanding recirculation zone, but rather is injected outside of a shrinking near wake so that it becomes exposed to the high speed convective flow.

As the escaping μspray begins to move rearward, it is itself accelerated, and this requires a small, but finite, amount of time. With a drag coefficient of unity, the equation of motion for a μspray drop is simply

$$\frac{du_c}{dt} = -\frac{3}{4}\frac{\rho_2}{\rho_\ell}\frac{u_c^2}{d_M} \quad , \tag{18}$$

in terms of the relative convective velocity, u_c. For the case of constant d_M, this integrates to

$$u_c = u_{c_o}\left(1 + \frac{3}{4}\frac{\rho_2}{\rho_\ell}\frac{u_{c_o} t}{d_M}\right)^{-1} \tag{19}$$

where u_{c_o} is the relative velocity at separation. Equation (19) provides an upper bound on acceleration times. For $u_{c_o} = u_2$, the time for a 10μ DECH drop to reach $u_c/u_{c_o} = 0.3$ is O(1 μsec) corresponding to $M_s = 4$, and $P_1 = 1$ atm oxygen; the time to reach $u_c/u_{c_o} = 0.1$ is O(5 μsec). Acceleration times scale linearly with μspray diameter.

The μspray that escapes at $t > t^*$ can be observed on streak photographs such as Fig. 15(b). Although the acceleration time of an escaped μspray drop is very short, it is largely converted to the vapor phase during that period. The 10μ DECH drop in the above example has a Weber number, $We = (\rho_2 u_c^2 d_M)/\sigma_\ell$, which is $O(10^3)$, and this is still far above the minimum Weber number that corresponds to the stripping mode,

We $\simeq 15$. If the stripping mechanisms are not essentially different than those for larger drops, the time for this 10μ drop to strip is $O(1\ \mu\text{sec})$. This is the same time order as its acceleration period. The "second generation" μspray produced during this stripping process, whose diameters should be $O(10^{-1}\mu)$, would vaporize in negligible time orders.

If the stripping mechanism is unacceptable for these small drop sizes, rapid conversion of the escaped μspray to the vapor phase can also be explained by convection assisted evaporation during the acceleration period. When the relative convective velocity is appreciable, as in the case of escaped μspray drops, the quiescent evaporation rate, given by Eq. (8), should be replaced with[22]

$$\frac{d\, d_M}{dt} = -\frac{C}{d_M}\left(1 + Re^{1/2}\, Pr^{1/3}\right) \quad , \tag{20}$$

in which $Re = (\rho_2\, u_c\, d_M)/\mu_2$, and $Pr = \mu_2 C_p/k$. The second term in brackets can account for a five-fold increase in evaporation rate under typical conditions, reducing the characteristic evaporation time of the 10μ diameter drop from 200 μsec to 40 μsec. Hence, if evaporation alone must account for the conversion of the μspray to vapor, an appreciable amount of this conversion can be shown to occur during the acceleration period.

It is most probable that both stripping and evaporation occur simultaneously. Neither appears to cause complete conversion of the μspray to vapor;

that is, the μspray remains visible on photographs. However, for modeling purposes, complete conversion will be assumed.

Under that assumption, the essential feature of the parent drop disintegration process, beginning at t*, is characterized by the impulsive continual injection of relatively large quantities of reactive vapor into the outer near wake region of the parent drop. This is somewhat similar to the occurrence of forward stagnation point mass addition as it might occur in a supersonic flow about a solid sphere or cylinder[23]. By that comparison, vapor concentrations can be expected to decrease with increasing axial and radial distance within the wake; the greater variation would be in the radial direction. In fact, the assumption of constant radial vapor distribution with increasing axial distance is not wholly unreasonable, over the first few diameters of length. On the other hand, an assumption of radial uniformity in the vapor concentration would appear to be a rather dangerous oversimplification.

Each local element of mixed fuel vapor and oxidizer may for modeling purposes be regarded as a homogeneous chemical system which, at the instant of initial mixing, has a specific mixture ratio and initial temperature. As reaction proceeds toward "equilibrium", the products remain within the element. Diffusion and thermal conduction between adjacent elements are ignored. The later was justified based on an estimate of laminar heat transfer over the time orders of interest. Each element therefore experiences an accelerated reaction rate due to self-heating. After an

induction time, τ_{chm}, the maximum rate of temperature rise is reached. The energy release rate at this time can be of explosive proportions; if so, it marks the point of wake ignition.

Now, the initial temperature in each element is a function of the vapor concentration there. That is, the maximum temperature of the fuel in the condensed phase is its boiling temperature at the prevailing local pressure. When the fuel changes phase and mixes with the oxidizer, the mixture temperature (assuming a mixing process which takes place at constant pressure) can readily be shown to be

$$T_i = \frac{T_b - \mathcal{L}/C_{pf}}{1+\alpha} + \frac{\alpha T_2}{1+\alpha} \quad , \tag{21}$$

in which T_b is the boiling point of the liquid, T_2 is the static temperature of the oxidizer in the free stream prior to mixing, and

$$\alpha = \left(\frac{1-\kappa_f}{\kappa_f}\right)\frac{C_{px}}{C_{pf}} \quad . \tag{22}$$

Here, κ_f is the mass fraction of fuel vapor in the element, and C_{px}, C_{pf} are the constant pressure specific heats of the fuel vapor and oxidizer, respectively.

The self-heating process is initiated at this temperature. To assess the duration of the induction period, the Edelman-Fortune global reaction rate equation for hydrocarbon vapor combinations with oxygen[24] is used. This is

$$\left.\frac{\partial C_f}{\partial t}\right|_{chm} = -5.52 \times 10^8 \, p^{-.825} \, T \, C_f^{1/2} \, C_{O_2} \exp\left[(-1.22 \times 10^4)/T\right] \quad , \quad (23)$$

in which C_f and C_{O_2} are the fuel and oxidizer concentrations in gram-moles/cm^3, while the units of system pressure and temperature are atmospheres and Kelvin degrees.

The induction period is assumed to proceed under a constant pressure condition. Thus, as heat is liberated by reaction, the element volume increases. Concentration changes are then due both to volumetric expansion and chemical reaction; the rate of energy liberation is determined from the latter. The fuel concentration in a constant pressure system can not be determined as a function of time from Eq. (23) alone. However, T(t) may be obtained from this expression directly, because $\rho = \rho(T)$, where ρ is the total element mass density.

For any hydrocarbon, the stoichiometric equation is

$$C_n H_m + (n + 1/4 \, m) \, O_2 - n \, CO_2 + 1/2 \, m \, H_2O \quad ,$$

and, temporarily assuming a fuel-lean system, the dissappearance rate of oxygen molecules is assumed to be approximately governed by this equation. Hence,

$$\left.\frac{\partial C_{O_2}}{\partial t}\right|_{chm} = n_s \left.\frac{\partial C_f}{\partial t}\right|_{chm} \quad , \quad (24)$$

in which $n_s = n + m/4$. Now for either species reactant, $C_i = \rho_i / w_i$, where ρ_i is its mass density and w_i its molecular weight. In terms of its mass fraction κ_i, this is $C_i = \kappa_i \rho / w_i$. Hence, Eq. (24) becomes

$$\frac{1}{w_{O_2}} \frac{\partial \kappa_{O_2}}{\partial t}\bigg|_{chm} = \frac{n_s}{w_f} \frac{\partial \kappa_f}{\partial t}\bigg|_{chm} \quad , \tag{25}$$

and also Eq. (23) may be rewritten in the form

$$\frac{1}{w_f} \frac{\partial \kappa_f}{\partial t}\bigg|_{chm} = -5.52 \times 10^8 \, p^{-.825} \, T \, \rho^{1/2} \, \frac{\kappa_f^{1/2} \, \kappa_{O_2}}{w_f^{1/2} \, w_{O_2}}$$

$$\cdot \exp\left[(-1.22 \times 10^4)/T\right] \quad . \tag{26}$$

Of course, mass fractions are not affected by simple volumetric expansion, and so Eq. (25) can be integrated to give

$$\kappa_{O_2} = \kappa_{O_{2_i}} - \frac{n_s \, w_{O_2}}{w_f} (\kappa_{f_i} - \kappa_f) \quad . \tag{27}$$

Note that in Eq. (26), the units of ρ are gram/cm^3.

Now, assuming a fuel lean condition, the heat of combustion per unit mass of fuel, $\mathcal{H}_c$, is approximately constant. Temperature increases due to combustion are then related to changes in quantity of fuel present through

$$d\kappa_f\Big|_{chm} = -\frac{C_p}{\mathcal{H}_c}\,dT \tag{28}$$

which is integrated to give

$$\kappa_f = \kappa_{f_i} - \frac{C_p}{\mathcal{H}_c}(T - T_i) \quad , \tag{29}$$

where C_p is the constant pressure specific heat of the mixture of gases in the element. Upon insertion of Eq. (29) in Eq. (27) we find

$$\kappa_{O_2} = \kappa_{O_{2_i}} - \frac{n_s w_{O_2} C_p}{w_f \mathcal{H}_c}(T - T_i) \quad , \tag{30}$$

Then, combining Eq. (26) and Eq. (28-30) there obtains, after changing units, the equation for temperature rise in the element,

$$\frac{dT}{dt} = k_4 \frac{T^{1/2}}{p^{.325}} \kappa_{f_i}^{1/2} \kappa_{O_{2_i}} \left[1 - \frac{C_p}{\kappa_{f_i}\mathcal{H}_c}(T - T_i)\right]^{1/2} \left[1 - \frac{n_s w_{O_2} C_p}{\kappa_{O_{2_i}} w_f \mathcal{H}_c}(T - T_i)\right] \cdot e^{-2.2\times10^4/T} \quad , \tag{31}$$

which is in terms of the initial concentrations in the wake, κ_{f_i} and $\kappa_{O_{2_i}}$. The constant k_4 has value

$$k_4 \equiv \frac{1.56 \times 10^{11}}{R^{1/2}} \left(\frac{w_f}{w_{O_2}}\right)^{1/2} \left(\frac{\mathcal{H}_c}{C_p}\right) \quad , \tag{32}$$

for which R is the specific gas constant of the mixture of gases in the element. Equation (31) has English system units.

From Eq. (31), we find the time for the temperature in the element to reach $\tilde{T}$ by integration, obtaining

$$\tau = \frac{p^{.325}\, E^{1/2}\, \psi(x_i)}{k_4\, \kappa_{f_i}^{1/2}\, \kappa_{O_{2_i}}} \quad , \tag{33}$$

where

$$\psi(x_i) \equiv \int_{x_i}^{\tilde{x}} \frac{e^{1/x}\, dx}{x^{1/2} \sqrt{1 - \theta_f (x - x_i)} \left[1 - \theta_{O_2} (x - x_i)\right]} \tag{34}$$

In this expression, $x = T/E$, $E = 2.2 \times 10^4\ ^oR$, and

$$\theta_f = \frac{C_p E}{\kappa_{f_i} \mathcal{H}_c}$$

$$\theta_{O_2} = \frac{n_s w_{O_2} C_p E}{\kappa_{O_{2_i}} w_f \mathcal{H}_c} \quad . \tag{35}$$

With $\tilde{T}$ properly chosen, the value of τ computed from Eq. (33) may be regarded as characteristic of the induction time which precedes very rapid reaction. For example, $\tilde{T}$ can be chosen as that temperature for which the integrand in Eq. (34) has its minimum. This would correspond to the moment of maximum rate of temperature rise, $(dT/dt)_{max}$.

Some simplification of Eq. (34) is possible by noting that $e^{1/x}/x^{1/2}$ decreases with extreme rapidity. For typical values of θ_f, θ_{O_2}, and x_i, the integrand, therefore, becomes very small before $\theta_f(x - x_i)$ or $\theta_{O_2}(x - x_i)$ become significant compared to unity. It suffices, in general, to approximate Eq. (34) with

$$\psi(x_i) \doteq \int_{x_i}^{\tilde{x}} \frac{e^{1/x}\,dx}{x^{1/2}} \quad , \tag{36}$$

in which x can be chosen as virtually any value for which $e^{1/x}/x^{1/2} \ll e^{1/x_i}/x_i^{1/2}$. Equation (36) is then a universal function of x_i only, whose values appear on Fig. 21.

Each element of reactive gases in the near wake of the parent drop begins at a temperature T_i (or x_i) from Eq. (21), and has an induction time given by Eq. (33). It is clear from Fig. 21 that $\psi(x_i)$, and therefore τ, is extremely sensitive to T_i, and this in turn is mainly a function of initial mixture ratio. The mixture ratio is not only spacially variable within the wake, but its distribution is also not duplicated in practice between parent drops that are subjected to identical conditions, as is apparent from photographs such as Fig. 22. In spite of this, measured ignition times[9,14] are reasonably reproducible, and so the sensitivity to the actual distribution of fuel vapor in the wake is apparently reduced by the mechanism of ignition that is involved.

An ignition mechanism which is consistent with these observations is as follows. It is postulated that "explosive ignition" of the entire near wake can be traced to homogeneous reaction which, occurring in a local reactive element, releases sufficient energy to produce a shock wave capable of initiating detonation in the remainder of the wake. For the present purpose, a simplistic initiation requirement will be assigned; namely, the local pressure rise must be equivalent to a Mach 3 shock wave.

The induction period of the homogeneous reaction was assumed to occur at constant pressure. However, once reaction rates become very large (i.e. $T \to \tilde{T}$), the process is better approximated by a constant volume assumption. If most of the temperature rise occurs at these high reaction rates, the total temperature rise is then simply

$$T_{max} - T_i = \frac{\mathscr{H}_c \kappa_f}{C_v} \quad , \tag{37}$$

which again assumes the fuel-lean condition, and C_v is the constant volume specific heat of the reactive element mixture. It is readily shown that if

$$\xi \equiv \frac{p_{max}}{p_i} - 1 \quad ,$$

the minimum mass fraction of fuel vapor required to produce a specified value of ξ is, from Eq. (37),

$$\kappa_f = \frac{T_i C_v \xi}{\mathcal{H}_c} \quad . \tag{38}$$

For the equivalent of a $M_s = 3$ shock, $\xi \simeq 9$.

It is easily shown that the initial value of C_v in the element is related to κ_f through

$$C_v = \kappa_f C_{v_f} [1 + \alpha(\gamma_f/\gamma_x)] \quad , \tag{39}$$

where γ_f and γ_x are the ratios of specific heats of the fuel vapor and oxidizer, and α is defined by Eq. (22). Combining Eq. (38) with Eq. (39) and (21), and assuming $\gamma_f/\gamma_x \simeq 1$ results in

$$\kappa_{f_{min}} \doteq 1/(1 + \omega) \quad , \tag{40}$$

where

$$\omega = \frac{C_{p_f}}{C_{p_x} T_2} \left(\frac{\mathcal{H}_c}{C_{v_f} \xi} + \frac{\mathcal{L}}{C_{p_f}} - T_b \right) \quad . \tag{41}$$

Elements with $\kappa_f < \kappa_{f_{min}}$ do not possess sufficient energy to produce the pressure rise corresponding to ξ, while elements with $\kappa_f > \kappa_{f_{min}}$ will require a longer induction time, because of their reduced T_i. By taking $\mathcal{H}_c(\kappa_f)$ into account for fuel rich mixtures, a corresponding maximum κ_f can be found in similar fashion, but the fuel-lean element will always ignite

first, due to its higher initial temperature. Hence $\kappa_{f_{min}}$ in Eq. (40) is used to compute the minimum chemical induction time prior to wake detonation.

It is noted that the mass fraction of fuel vapor corresponding to the stoichiometric condition is easily found to be

$$\kappa_f^* = \frac{\lambda \phi_o^*}{1 + \lambda \phi_o^*} \quad , \tag{42}$$

in which ϕ_o^* is the stoichiometric fuel-oxygen mass ratio, and λ is the initial mass fraction of oxygen in the oxidizer gas. If $\kappa_{f_{min}} > \kappa_f^*$, explosive ignition is not possible; i. e. more energy is needed to initiate detonation than is available in any reactive element. Each element will proceed with local homogeneous reaction. This is also what should occur in elements having $\kappa_f < \kappa_{f_{min}}$, which pass through (dT/dt_{max}) prior to τ, and explains the appearance of luminous turbulent regions in the wake, which occur before explosive ignition is observed, cf. Fig. 20.

C. Results and Discussion

The time to explosive wake ignition, measured from first contact by the incident shock with the parent drop, is prescribed to be

$$t_{ig} = t^* + \tau_{chm} \tag{43}$$

in which t* is the time to reach peak frontal diameter; namely,

$$t^* = (D_o \overline{T}^*)/(u_2 \beta^{1/2}) \quad , \tag{44}$$

and τ_{chm} is obtained from Eq. (33) and (36) using $\kappa_{f_{min}}$ from Eq. (42) to compute T_i in Eq. (21). The results from this computation are compared with experimental data on Fig. 23-25, showing the effects of Mach number, initial oxidizer pressure, and parent drop size.

The phenomenological description given here is not applicable to shock wave interactions with parent drops under conditions which would produce first generation μspray whose characteristic quiescent evaporation times are significantly less than t*. In such a case, explosive ignition within the recirculation zone, prior to t*, is conceptually possible. Under typical conditions, this roughly restricts the present formulation to $D_o > 100\mu$. It should also be pointed out that the chemical induction time is quite sensitive to the liquid boiling temperature, T_b, through its effect on T_i, while accurate high temperature boiling point data is not available for all hydrocarbons. Moreover, the Edelman-Fortune reaction rate equation is strictly applicable to hydrocarbons (both olefin and parafin), and to the approximate temperature range $1440 < T < 5400\ ^oR$. Other reaction rate expressions must be used to derive induction time expressions similar to Eq. (33) for other fuels and temperature ranges.

2. Self Oxidizing, Bi-Liquid (SOBL) Spray Detonations

All of our earlier work on heterogeneous detonation was concerned with liquid fuel drops distributed in a gaseous oxidizer. In these studies it was found that such detonations are relatively easy to generate. The interest of this extension, then, was to investigate the possibility of detonation in a system comprised of liquid fuel drops, liquid oxidizer drops, and an inert gas. In such systems there exists the possibility of realizing much higher pressures, the limit being those associated with condensed detonations as the inert gas concentration approaches zero. In order that SOBL detonations be realized, it is required that the shock wave create a microspray in the wake of the fuel and oxidizer drops, that this spray evaporates and mixes with the other species, and, further, that all of this occurs rapidly enough that heat and momentum losses to the walls of the detonation tube don't preclude ignition. The necessity of mixing the wakes of the fuel and oxidizer drops implies that the reaction zone length will be much longer, that wall effects will be more pronounced, and hence that detonation will be more difficult.

Kerosene and concentrated hydrogen peroxide (50%) were chosen for the liquids with the gas being nitrogen. The vertical detonation tube, 1 5/8 in. by 1 5/8 in. and 12 ft long, was used for these studies. Extensive modifications were made to the drop generator so that the desired drop sizes and amounts for the two different liquids could be accommodated.

Further, a blast wave driver was added to the bottom of the vertical tube so that a strong blast wave could impact the heterogeneous mixture. The blast wave was generated by the detonation of H_2 and O_2 at initially elevated pressures.

Hydrogen peroxide (50%) is a strong oxidizer which presented difficult storage and handling problems, particularly when used in the drop generating system. The dissociation of H_2O_2 led to safety problems (and one accident) and also upset the requisite hydraulic character of the drop generating system. However, these problems were finally overcome and the experiments conducted.

An analysis was performed to guide the experiments and particular attention was given to the global equivalence ratio, the ratio of the diameter of fuel drops to that of the oxidizer drops, and the ratio of the maximum interaction distance of the two liquids to the hydraulic radius of the tube. While difficult to judge in some cases, the conclusion reached was that detonation was not realized. However, these studies were not all inclusive and it is believed that SOBL detonations can be generated under the appropriate conditions and further investigation is warranted. Stronger peroxide solutions, other liquid combinations, smaller drop sizes, and larger detonation tube cross section would be appropriate steps in this direction. A complete write up on this investigation is being prepared for publication and should be available in the near future.

REFERENCES

1. Nicholls, J.A., "Two Phase Detonation Studies Conducted in 1971," NASA CR 120924, NASA Contractors Report, April 1972.

2. Nicholls, J.A. et al., "Two Phase Detonation Studies Conducted in 1972," UM 026030-4-P, The University of Michigan, March 1973.

3. Nicholls, J.A. and Miyajimi, H., "Interaction of a Shock Wave with a Burning Drop," presented at Third International Symposium on Combustion Processes, September 24-27, 1973, Kazimierz nad Wisla, Poland.

4. Ranger, A.A. and Nicholls, J.A., "Atomization of Liquid Droplets in a Convective Gas Stream," Int. J. Heat Mass Transfer, Vol. 15, 1972, p. 1203 ff.

5. Ranger, A.A. and Nicholls, J.A., "Aerodynamic Shattering of Liquid Drops," AIAA J., Vol. 7, No. 2, February 1969.

6. Reinecke, W.G. and Waldman, G.D., "An Investigation of Water Drop Disintegration in the Region Behind Strong Shock Waves," Third International Conference on Rain Erosion and Related Phenomena, August 1970.

7. Aeschliman, D.P., "An Experimental Study of the Response of Water Droplets to Flows Behind Plane Shock Waves," Sandia Lab. Res. Report No. SC-RR-71 0540, 1971.

8. Reinecke, W.G. and McKay, W.L., "Experiments on Water Drop Breakup Behind Mach 3 to 12 Shocks," Sandia Lab. Res. Report No. SC-CR-70-6063, 1969.

9. Kauffman, C.W. and Nicholls, J.A., "Shock-Wave Ignition of Liquid Fuel Drops," AIAA J., Vol. 9, No. 5, May 1971, pp. 880 ff.

10. Lu, P.L. and Slagg, N., "Chemical Aspects of the Shock Initiation of Fuel Droplets," Picatinny Arsenal, AMCMS Code 552C.12.559, 1971.

11. Kauffman, C.W., Nicholls, J.A., and Olzmann, K.A., "The Interaction of an Incident Shock Wave with Liquid Fuel Drops," Combustion Science and Technology, Vol. 3, No. 4, 165 (1971).

12. Berger, S.A., Laminar Wakes, Amer. Elsevier, New York, 1971.

13. Fishburn, B.D., "Boundary Layer Stripping of Liquid Drops Fragmented by Taylor Instability," Fourth International Colloquium on Gasdynamics of Explosions and Reactive Systems, 1973.

14. Kauffman, W.C., "Shock Wave Ignition of Liquid Fuel Drops," Ph.D. Thesis, Univ. of Michigan, 1971.

15. Pierce, T.H., "Experimental and Theoretical Study of the Structure of Two-Phase Detonation in Sprays," Ph.D. Thesis, Univ. of Michigan, 1972.

16. Fishburn, B.D., private communication, 1973.

17. Ranger, A.A., "Shock Wave Propagation Through a Two-Phase Medium," Astronautica Acta, Vol. 17, 1972, pp. 675 ff.

18. Dabora, E.K., "Production of Monodisperse Sprays," Rev. Scientific Instruments, Vol. 38, No. 4, 1967, pp. 502 ff.

19. Collins, R. and Charwat, A.F., "The Deformation and Mass Loss of Liquid Drops in a High-Speed Flow of Gas," Israel J. of Technology, Vol. 9, No. 5, 1971, pp. 453 ff.

20. Dabora, E.K., Ragland, K.W., and Nicholls, J.A., "Detonations in Two Phase Media and Drop Shattering Studies," NASA CR-72421, May 1968.

21. Williams, F.A., "Progress in Spray-Combustion Analysis," Eighth Symposium (International) on Combustion, Williams and Wilkins Co., Baltimore, 1962.

22. Williams, F.A., Combustion Theory—The Fundamental Theory of Chemically Reacting Flow Systems, Addison-Wesley Publ. Co., Inc., 1965, p. 57.

23. Collins, D., Lees, L., and Roshko, A., "Near Wake of a Hypersonic Blunt Body with Mass Addition," AIAA J., Vol. 8, No. 5, 1970.

24. Edelman, R.B., Fortune, O., and Weilerstein, G., "Some Observations on Flows Described by Coupled Mixing and Kinetics," Emissions from Continuous Combustion Systems, Plenum Press, N.Y., 1972.

BIBLIOGRAPHY

Publications Arising from Grant NGL 23-005-336

Nicholls, J.A., "Two Phase Detonation Studies Related to Rocket Instability—1969," NASA CR 72668, March 11, 1970.

Nicholls, J.A., "Two Phase Detonation Studies Conducted in 1970," NASA CR 72866, March 1971.

Nicholls, J.A., "Aerodynamic Shattering and Combustion of Fuel Drops and Films in I.C. Engines," presented at Spring 1971 Meeting, Engines and Emissions, Central States Section, The Combustion Institute, Ann Arbor, Michigan, March 23, 24, 1971.

Kauffman, W.C. and Nicholls, J.A., "Shock Wave Ignition of Liquid Fuel Drops," AIAA J., Vol. 9, No. 5, May 1971, pp. 880-885.

Kauffman, W.C., Nicholls, J.A., and Olzmann, K., "The Interaction of an Incident Shock Wave with Liquid Fuel Drops," Combustion Science and Technology, Vol. 3, 1971, p. 165.

Sichel, M., Rao, C., and Nicholls, J.A., "A Simple Theory for the Propagation of Film Detonations," Thirteenth Symposium (International) on Combustion, The Combustion Institute, Pittsburgh, Pennsylvania, 1971, pp. 1141-49.

Pierce, T.H., "Production of Polydisperse Sprays," The Review of Scientific Instruments, Vol. 42, No. 11, November 1971, pp. 1648-49.

Nicholls, J.A., "Two Phase Detonation Studies Conducted in 1971," NASA CR 120924, April 1972.

Nicholls, J.A. and Sichel, M., "Detonation of Liquid Fuel Drops and Films," presented at the Second Conference on Natural Gas Research and Technology, 5-7 June 1972, Atlanta, Georgia, in proceedings.

Pierce, T.H. and Nicholls, J.A., "Time Variation in the Reaction Zone Structure of Two Phase Spray Detonations," presented at the 14th International Symposium on Combustion, Pennsylvania State University, August 1972.

Pierce, T. H. and Nicholls, J. A., "Two Phase Detonations with Bimodal Drop Distributions," Third International Colloquium on Gasdynamics of Explosions and Reactive Systems, University of Marseille, France, 12-17 September 1971. Astronautica Acta, Vol. 17, Nos. 4 and 5, 1972, pp. 703-713.

Rao, C., Sichel, M., and Nicholls, J. A., "A Two Dimensional Theory for Two Phase Detonation of Liquid Films," Combustion Science and Technology, Vol. 4, 1972, pp. 209-220.

Ranger, A. A. and Nicholls, J. A., "Atomization of Liquid Droplets in a Convective Gas Stream," International Journal of Heat and Mass Transfer, Vol. 15, 1972, pp. 1203-1211.

Shen, Peter I-wu and Adamson, T. C., Jr., "Theoretical Analysis of a Rotating Two-Phase Detonation in Liquid Rocket Motors," Astronautica Acta, Vol. 17, 1972, pp. 715-728.

Shen, I-wu and Adamson, T. C., Jr., "Theoretical Analysis of a Rotating Two Phase Detonation in a Rocket Motor," NASA CR 121194, March 1973.

Nicholls, J. A. and Miyajima, H., "Interaction of a Shock Wave with a Burning Drop," presented at Third International Symposium on Combustion Processes, Polish Academy of Sciences, September 1973, to be published in Archives of Combustion Processes, Warsaw, Poland.

Pierce, T. H. and Nicholls, J. A., "Hybrid Gas-Phase/Two-Phase Detonations," accepted for publication in Combustion Science and Technology.

Wierzba, A. S., Kauffman, C. W., and Nicholls, J. A., "Ignition of Partially Shattered Liquid Fuel Drops in a Reflected Shock Wave Environment," accepted for publication in Combustion Science and Technology.

APPENDIX A—DROP GENERATOR POWER REQUIREMENTS

1. THEORY

A. Power and Amplitude of Disturbance

Consider a jet of fluid emerging from a vertically mounted capillary tube in a coordinate system moving at the same velocity as the jet. Prior to the application of any disturbance the fluid inside the stationary column (which is what the jet appears to be) has a pressure which exceeds the ambient pressure by an increment attributable to the surface tension. This increment is inversely proportional to the jet radius. Hence if the pressure in the jet is made to vary in a regular manner by some means, variations in jet radius and jet instability may result. Rayleigh[1] showed that for a given jet diameter the disturbance wavelength for which the amplitude will grow most rapidly is given by,

$$\lambda_R = 4.508\, d_j \tag{1}$$

where λ_R is the wavelength of the disturbance with maximum growth rate

d_j is the diameter of the jet

The wavelength, frequency and jet velocity are related by,

$$\lambda = u_j/f$$

or from Eq. (1)

$$f_R = u_j/4.508\, d_j \tag{2}$$

where f_R is the frequency for maximum disturbance growth rate, the Rayleigh frequency

u_j is the jet velocity

Equating the volume of a drop to that contained in one wavelength

$$\frac{\pi}{6} D_0^3 = \frac{\pi}{4} \lambda d_j^2$$

The jet diameter may be replaced by the capillary diameter without appreciable error to give

$$D_0/d_t = 1.89 \tag{3}$$

where D_0 is the drop diameter

d_t is the capillary (or needle) diameter

For a jet of liquid of viscosity μ_l, density ρ_l, and surface tension σ injected into an atmosphere of viscosity μ_g and density ρ_g, an expression for the minimum power required for jet breakup[2] is,

$$\overline{P}_{min} = \frac{\pi m r^3 \sigma^2}{64 \nu_\ell^3 r_t^2 L^2} \rho_\ell^2 f^2 e^{(-2qx/u_j)} \tag{4}$$

where (see Fig. A-1) the needle (capillary) is mounted in a fixed platform, P_2, and is connected to the supply tank through a supply tubing, part of which is mounted on a platform, P_1, of mass, m, being vibrated at frequency f.

$\overline{P}_{min}$	average minimum power required for jet breakup
m	mass of vibrated assembly
r	radius of vibrated tube
L	length of vibrated tube
ν_ℓ	kinematic viscosity of the liquid
ρ_ℓ	density of the liquid
σ	surface tension of the liquid
f	frequency of vibration
q	growth parameter in Rayleigh's analysis
x	breakup distance from needle tip $= \theta x_n$
x_n	natural breakup distance
θ	x/x_n

The natural breakup distance is the distance in which the jet would disintegrate naturally without a force disturbance being applied. Grant and Middleman[3] presented a comprehensive study and observed that for a fixed jet size d_t, the breakup distance is a function of jet velocity u_j and has a maximum at the point $u_j = u_j^*$. For $u_j < u_j^*$

$$\frac{x_n}{d_t} = 19.5\ (We^{1/2} + 3\ We/Re)^{0.85} \qquad (5)$$

where We is the Weber number $= (\rho_\ell\ u^2\ d_t/\sigma)$

Re is the Reynolds number $= (\rho_\ell\ u\ d_t/\mu_\ell)$

also u_j^* corresponds to the condition,

$$Re^* = 325\ (Z^*)^{-0.28}$$

where Re^* is the Reynolds number corresponding to u_j^*

Z^* is the Ohensorge number $(We^{1/2}/Re)$ corresponding to u_j^*

For $u_j > u_j^*$ or $Re > Re^*$, x_n/d_t cannot be evaluated in a closed form and an iteration procedure has to be used[2].

Since the power required depends on the mass of the assembly, which will depend on the kind of apparatus used, a more useful parameter is the amplitude of vibration, A, which is coupled to the power, $\overline{P}$, through a simple relation for a sinusoidal disturbance,

$$A^2 = \frac{\overline{P}}{8\pi^2\, mf^3} \tag{6}$$

combining Eqs. (4) and (6)

$$A_{min} = \frac{\beta\sigma\, r^2\, e^{-qx/u_j}}{16\sqrt{2}\,\pi\mu\, r_t\, Lf} \tag{7}$$

$$\beta = \left(\frac{\pi f \rho r^2}{\mu}\right)^{1/2} \tag{8}$$

The pressure perturbations produced in the liquid as a result of the vibrations are given by

$$P' = \frac{16\sqrt{2}\,\pi\,\mu_\ell\,ALf}{\beta\,r^2}$$

$$\frac{P'}{P_0} = \frac{16\sqrt{2}\,\pi\,\mu_\ell\,ALf}{P_0\,\beta\,r^2} \tag{9}$$

where P_0 is the atmospheric pressure.

B. Dimensional Analysis

The important variables are d_t, u_j, and ρ_ℓ, which will be used as repeated variables along with d, L, A, μ_ℓ, σ, and x. This leads to the dimensionless parameters

$$\pi_1 = d/d_t \quad , \quad \pi_2 = L/d_t \quad , \quad \pi_3 = A/d_t$$

$$\pi_4 = (u_j/d_t f) = 4.508 \text{ (for } f = f_R) \quad , \quad \pi_5 = (\rho_\ell\, d_t\, u_j/\mu_\ell) = Re$$

$$\pi_6 = (\rho_\ell\, d_t\, u_j^2/\sigma) = We \quad , \quad \pi_7 = x/d_t$$

Then from Eqs. (7) and (8), a straightforward substitution gives

$$\beta = \pi_1 \left(\frac{\pi_5 \cdot \pi}{4\pi_4}\right)^{1/2} \tag{10}$$

and

$$\pi_{3min} = \frac{K_1\,(\pi_5)^{3/2}}{(\pi_6)} \cdot e^{-\left[\frac{0.948\,\pi_7}{(\pi_6)^{1/2}}\right]} \tag{11}$$

where

$$K_1 = \frac{\pi_1 (\pi_4)^{1/2}}{64 \sqrt{2\pi}\ \pi_2} \tag{12}$$

Now to study the dependence of amplitude on other variables, ideally it is necessary to vary one while holding all others constant. In the experiment reported here the ratios π_1 and π_2 were kept constant ($\pi_1 = 2$, $\pi_2 = 37$). Also, since it was desirable to operate at f_R for any velocity u_j, π_4 was also a constant at a value 4.508. Then Eq. (11) predicts the dependence of π_3 on π_5, π_6, and π_7.

2. EXPERIMENTAL ARRANGEMENT

A. Apparatus

Apparatus reservoir R contained prefiltered test liquid. It was pressurized (usually to a constant 30 psig pressure) using a nitrogen bottle S. The supply manifold consisted of 1/4 in. ID clearflow tubing up to the coarse metering valve C_2 and 0.065 in. ID Teflon tubing from C_2 to the vibrated tube N_1 and from N_1 to the stationary capillary (needle) N_2.

The platform P_2 was attached to a M. B. Manufacturing Co. (Model 631H) shaker 'V' which was excited by an audio oscillator (HP Model 2020) and an amplifier (MB, Model 1132034). The platform vibrations were sensed using a 6 mv/g sensitivity accelerometer, A (Metrex Inst. Co. Model 512-1). The accelerometer output and the vibrator input current (for testing its sinusoidality) were displayed on a dual beam oscilloscope, O.

The pressure drop across N_2 was measured using a zero volume Micro Systems pressure transducer. The pressure transducer output was displayed on a Fluke 8300 A DVM. The sensitivity was 1.95 mv/psi. The breakup pattern was observed using a General Radio Co. Strobotac Type 1531-A.

The shaker was mounted on isolation mounts to isolate the shaker and the rest of the system. The entire system was kept in a room maintained at $70^{\circ}F$ to eliminate any temperature variation effects on viscosity and other parameters.

B. Measurements and Calibration

It was necessary to obtain a calibration of pressure drop across the needle (measured by transducer PT) against the average jet velocity. This was done by measuring the mass flux through the needle (for all test liquids) for various pressure settings. Since the needle diameter was fixed and the measurements were to be made at the Rayleigh frequency*, this calibration could be converted to a P_{set} vs frequency curve.

Since the amplitudes of vibration involved were extremely small they were not measured directly. Instead the acceleration of the platform was measured using the accelerometer A. The output of the accelerometer

*For a given frequency, various settings of pressure drop were tried and the one corresponding to minimum power was found to be approximately the same as predicted by Rayleigh.

was directly measured on the scope and the acceleration amplitude was converted to vibration amplitude knowing the frequency of vibration. They are coupled by

$$a = 4\pi^2 \cdot f^2 \cdot A \tag{13}$$

where a is the amplitude of acceleration.

The power measurements were made for various frequencies with the pressure drop (or velocity) corresponding to that which was found from the previously made operating curve. Measurements were made only up to the point beyond which either the power supplied by the amplifier or the vibrations (as depicted by the accelerometer output on the scope) were no longer sinusoidal.

Once the flow rate was adjusted for a given frequency, the power was gradually increased until a uniform string of drops was produced. When the stroboscope is used as a source of light to view the breakup pattern, a uniformly broken jet produces a stationary pattern of drops as in Fig. A-2. When the power is slightly reduced the disturbance introduced is incapable of producing uniform drops, even though it still breaks up the jet as can be seen from Fig. A-3. When the power is completely shut off the jet breaks up "naturally" and since an ordinary lamp was used as a light source for this part, the long exposure time produces the apparent multi-exposure pattern shown in Fig. A-4.

The patterns such as in Fig. A-2, were taken as acceptable and the minimum power required to produce them was recorded. If the power is increased beyond this value no significant changes take place in the appearance of the pattern except that the point where the jet begins to breakup shifts towards the needle, i.e. the breakup distance x is reduced.

It was also observed that the breakup distance, x, corresponding to the acceptable breakup pattern is always less than the natural breakup distance, x_n. However, these distances were not measured.

3. CHOICE OF PARAMETERS AND RESULTS

A. Choice of Liquids and Tube Sizes

TABLE A-1. PHYSICAL PROPERTIES OF LIQUIDS TESTED*

No.	Substance	Density Slugs/ft^3	Viscosity lb-sec/ft^2	Surface Tension lb/ft
1	Kerosene	1.44	3.44×10^{-5}	1.94×10^{-3}
2	Ethyl Alcohol	1.52	2.50×10^{-5}	1.50×10^{-3}
3	Benzene	1.74	1.31×10^{-5}	1.98×10^{-3}
4	Water	1.94	2.09×10^{-5}	5.01×10^{-3}

*Actual measurements for the sample were used for kerosene. Otherwise the source was the Handbook of Chemistry and Physics.

The liquids were chosen so as to have pairs in which the two liquids had all properties approximately the same except one. Thus, for viscosity, the pair is benzene and Kerosene, and for surface tension, alcohol and water.

The power is extremely sensitive to the needle diameter (see Ref. 2, p. 236) and hence a needle diameter of 0.027 in., which produced 1300 μm drops (see Eq. (3)) and which required a reasonable amount of power for the chosen frequency range, was selected.

For all liquids except water the tests were carried out at this needle diameter. For water an additional needle of 0.039 in. diameter was used. The length of the needles was 2 in and they were made by telescoping two or three stainless steel tube pieces to give an OD of 0.016 in. to fit the supply tubing and the required ID. The vibrated tube was mounted on P_1 (Fig. A-1) and had an ID of 0.054 in. and was 1 in. in length. The supply tubing downstream of C_2 was flexible enough so as not to resist the vibrations. The entire fuel system was maintained hydraulic so as to obtain instantaneous response to any changes in flowrate (using either C_2 or C_3).

B. Results

From the recorded data, values of the various parameters, $\pi_1 - \pi_6$, were calculated. Because of the choice of needle diameter and Rayleigh frequency, π_1, π_2, and π_4 were constant throughout except for water. Thus,

$$\pi_1 = 2.0 \quad , \quad \pi_2 = 37.0 \quad , \quad \pi_4 = 4.508$$

for all liquids. In addition, for water,

$$\pi_1 = 1.385 \quad , \quad \pi_2 = 25.6 \quad , \quad \pi_4 = 4.508$$

From measured values of parameters π_1 - π_6, the values of π_7 were calculated using the relation:

$$\pi_7 = \frac{(\pi_6)^{1/2}}{0.948} \log \frac{K_1 (\pi_5)^{3/2}}{\pi_6 \cdot \pi_3} \qquad (14)$$

which is just an inversion of Eq. (11).

Values of (x_n/d_t) were calculated using Eq. (5), or iteration procedure, as appropriate for the same conditions knowing the Re and We (i.e. π_5 and π_6) and from this values of $\theta = (x/x_n)$ were obtained.

Also, the values of P'/P_0 were calculated from Eq. (9), using from the measured or known values. These values of π_3, π_5, π_6, π_7, (x_n/d_t), θ, and P'/P_0 are tabulated in Table A-2.

Comparing the values of π_7 and (x_n/d_t) it can be easily seen that $\pi_7 < (x_n/d_t)$. This is an expected result, since the externally introduced disturbance should break up the jet earlier than if it were broken up naturally. In fact, this is the reason why any external power is needed at all. This is in agreement with the previously recorded observation that increase of power after the minimum point merely results in reducing the breakup distance. The regularity of the disturbance results in a regular breakup pattern.

Thus in Eq. (4), x can be replaced by $\theta \cdot x_n$, which is a modification of the original equation from Ref. 2. Note that the only way to substitute a

meaningful distance x from a purely theoretical basis is by relating it to the natural breakup distance. Thus, the original equation in Ref. 2 could be looked upon as a zeroth order approximately where the a priori assumption, $x = x_n$, was made. However, as explained above, it would be expected that $(x/x_n) < 1$, always.

It can also be seen from Table A-2 that the value of θ varies between 0.4 and 0.8, being very close to 0.8 for many readings. Therefore, the average value of $\theta = 0.58$ was chosen to relate x with x_n. This could be taken as a first approximation. With this x the values of $\pi_3 = A/d_t$ were calculated theoretically and are tabulated in the last column of Table A-2. The experimental values are compared with theory in Figs. 5 and 6 for the four liquids tested. The disagreement for some points is considerable, particularly when θ takes extreme values like 0.4 and 0.8. This is due to the exponential dependence of π_3 on π_7 (i.e. θ). From the values of P'/P_0, appearing in Table A-2, it can be seen that the pressure perturbations produced are indeed very small and are comparable with those in an audible sound wave. This justifies the small perturbation assumptions made in deriving Eq. (9), and others.

4. DISCUSSION

It seems that a better correlation between the actual breakup distance x and the natural one x_n, i.e. the value of parameter θ and its dependence on flow parameters like Re and We determined from actual experimental

measurements, would improve the accuracy of the theoretical predictions of required minimum amplitude (or power) considerably. It is believed that this uncertainty is the largest contributor to the discrepancy between experiment and theory. Further investigation is required.

It should also be noted that the analysis presented here could be used irrespective of the method of introducing the disturbances, provided they are introduced axially.

TABLE A-2. TABULATED RESULTS

π_3 x 10^{-4}	π_5	π_6	π_7	x_n/d_t	$\theta = x/x_n$	P'/P_0 x 10^{-6}	Theo. π_3 x 10^{-4}
0.638	576.0	61.9	64.94	130.6	0.50	0.323	0.168
0.749	672.0	84.3	73.48	141.9	0.52	0.409	0.292
0.720	768.0	110.1	83.67	149.4	0.56	0.421	0.538
0.797	864.0	143.2	93.01	153.0	0.61	0.507	1.095
0.645	960.0	172.0	104.56	153.1	0.68	0.421	1.972
1.30	1056.0	208.0	103.66	152.5	0.68	0.886	3.418
1.79	1152.0	247.6	107.05	151.9	0.70	1.276	5.49
2.31	1248.0	290.7	110.59	151.5	0.71	1.724	8.04
4.23	1342.5	337.1	106.68	151.1	0.70	3.272	10.97
4.70	1440.0	387.0	111.42	150.7	0.73	3.758	14.74
6.48	1536.0	440.3	111.04	150.4	0.73	5.348	18.67
10.4	920.0	37.3	40.22	108.4	0.38	1.222	0.303
4.87	1380.0	83.9	65.70	134.8	0.49	0.700	1.31
6.57	1670.0	114.2	72.39	138.9	0.52	1.021	3.12
7.61	1840.0	149.1	79.97	138.6	0.58	1.264	7.25
6.48	2070.0	118.1	77.72	138.0	0.56	0.713	5.17
6.40	2300.0	233.0	100.97	137.6	0.73	1.187	23.4
6.69	2530.0	281.9	109.43	137.2	0.79	1.302	35.6
7.99	2760.0	335.5	115.12	136.9	0.80	1.623	49.9
10.89	844.0	14.4	28.10	74.0	0.38	1.861	0.263
17.46	1055.0	22.5	32.20	85.0	0.38	3.337	0.561
17.85	1266.0	32.4	37.96	92.0	0.41	3.737	1.34
10.79	1688.0	57.6	53.49	94.9	0.56	2.608	8.61
16.97	1879.0	72.9	55.43	94.7	0.58	4.420	17.6
168.7	3165.0	202.5	54.30	94.2	0.58	55.837	165.4
416.0	4220.0	360.0	51.46	94.0	0.55	159.0	357.4
0.40	906.0	18.3	45.98	79.0	0.58	0.031	0.416
44.7	1208.0	32.5	32.05	90.1	0.36	4.01	2.12
25.7	1510.0	50.8	43.40	92.3	0.47	2.578	6.53
15.2	1812.0	73.1	55.98	92.7	0.60	1.669	19.14

REFERENCES

(for Appendix A)

1. Rayleigh, J.W.S., "On the Instability of Jets," Proc. London Math. Soc., Vol. 10, 1878.

2. Pierce, T.H., "Experimental and Theoretical Studies of the Structure of Two-Phase Detonation in Sprays," Ph.D. Thesis, Univ. of Mich., 1972.

3. Grant, R.P. and Middleman, S., "Newtonian Jet Stability," AICh. E.J., Vol. 12, No. 4, July 1966.

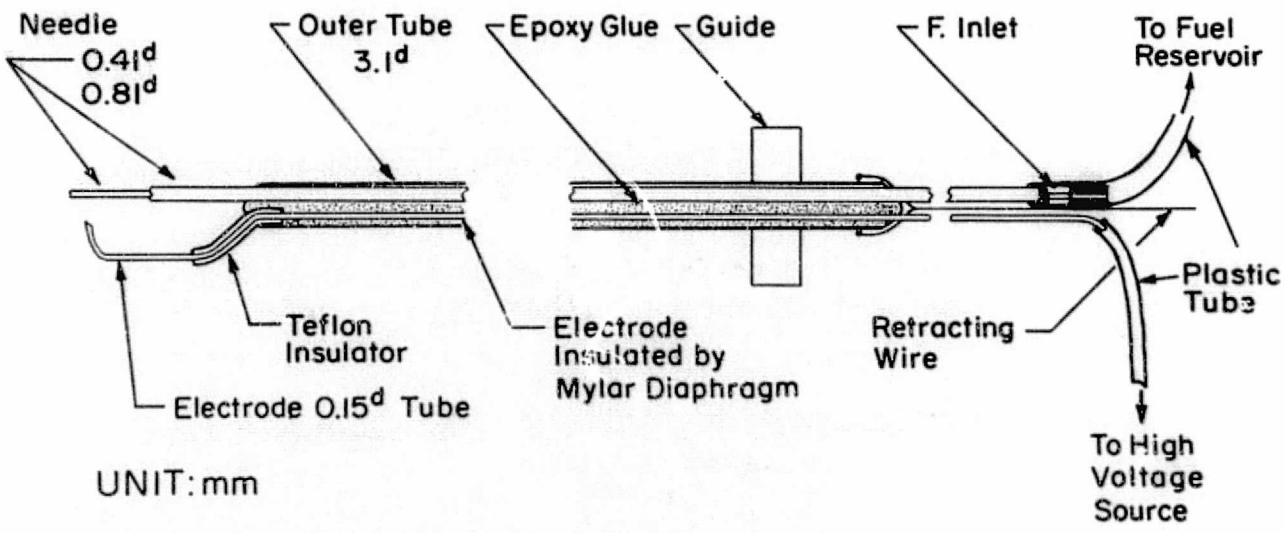

Figure 1. Needle-Electrode Assembly.

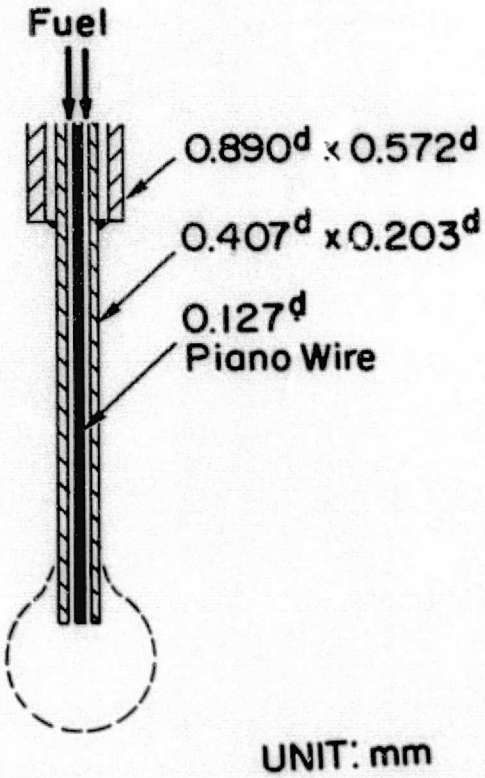

Figure 2. Needle Tip Configuration.

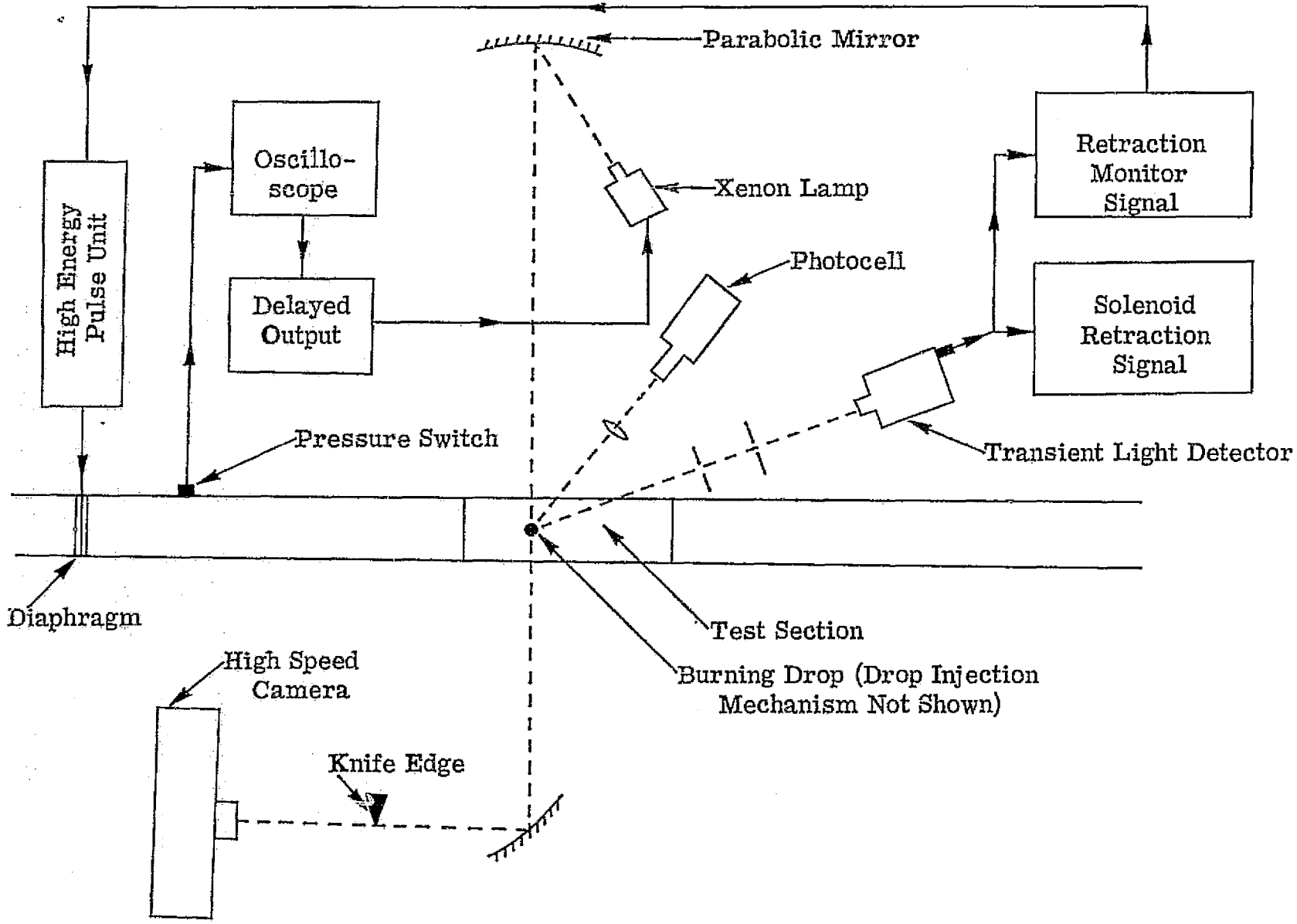

Figure 3. Equipment Arrangement.

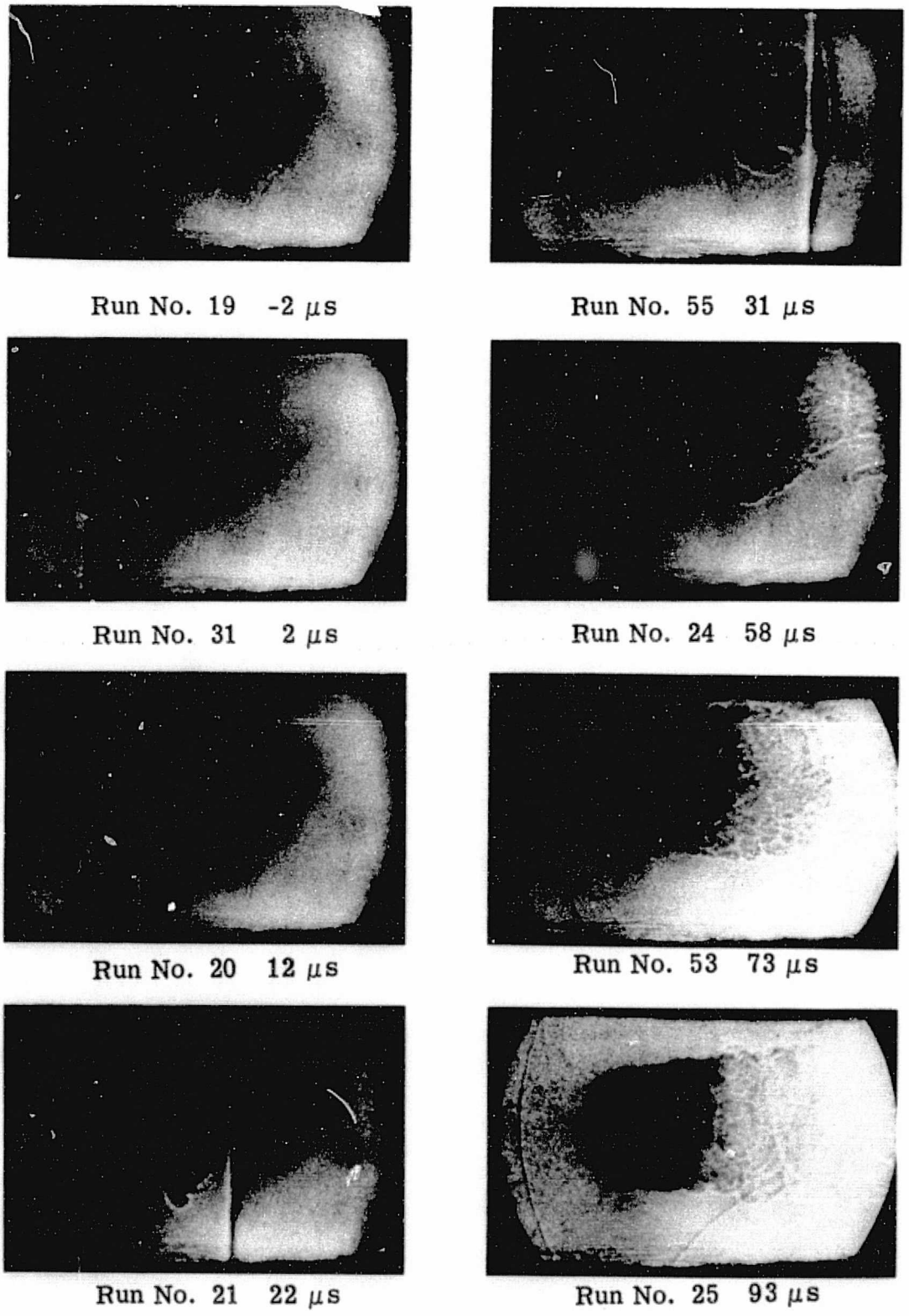

Run No. 19 -2 μs

Run No. 55 31 μs

Run No. 31 2 μs

Run No. 24 58 μs

Run No. 20 12 μs

Run No. 53 73 μs

Run No. 21 22 μs

Run No. 25 93 μs

Figure 4. Shock Wave Interaction of Initially Ignited Drops, P_1 = 30 in. Hg O_2, M_s = 2.02, d_o = 1.6 mm.

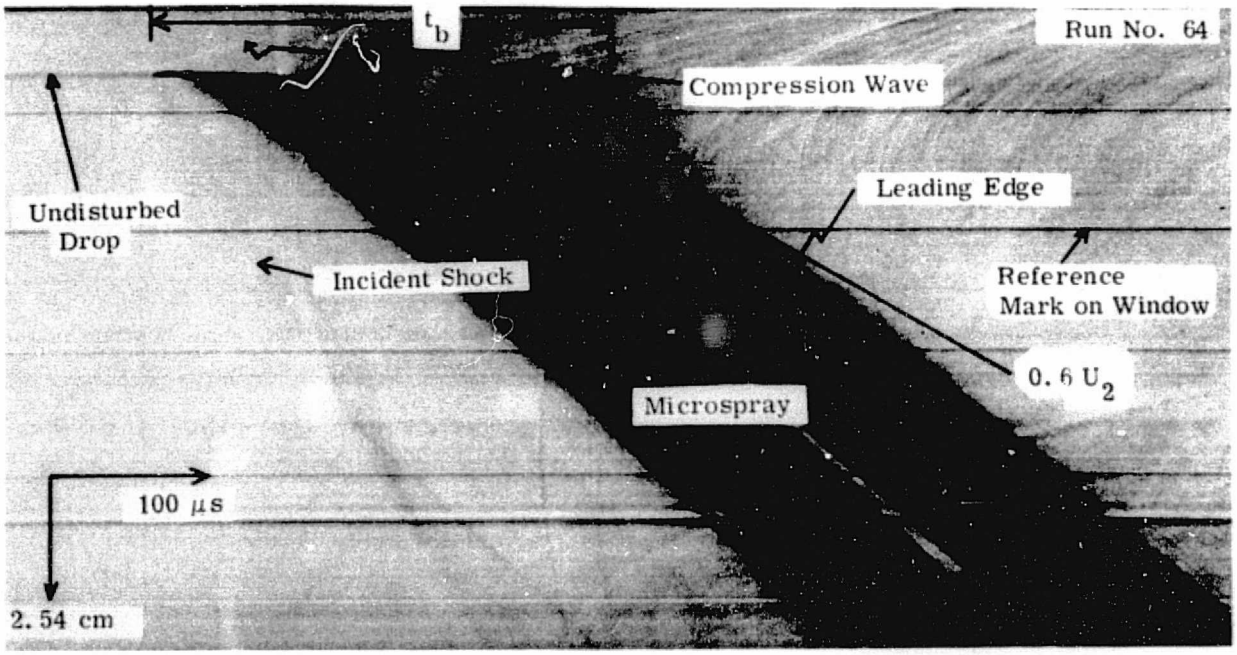

Figure 5. Streak Schlieren Photograph of Non-ignited Drop, P_1 = 30 in. Hg O_2, M_s = 1.73.

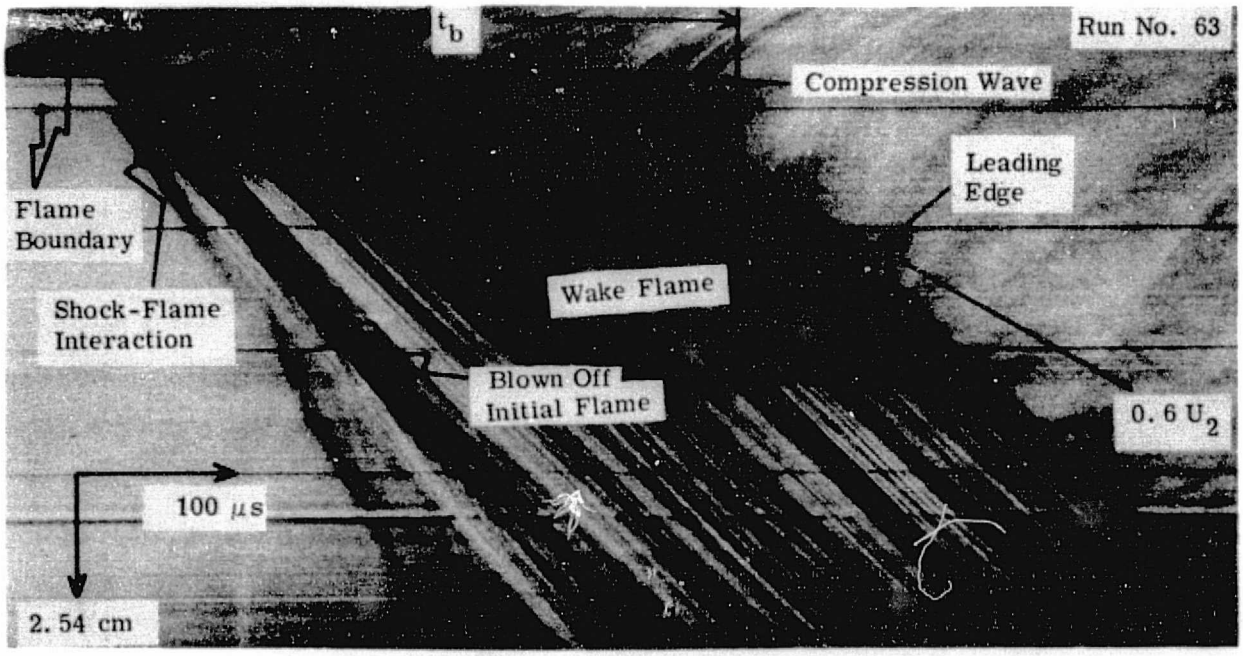

Figure 6. Streak Schlieren Photograph of Drop with Wake Flame, P_1 = 30 in. Hg O_2, M_s = 1.72.

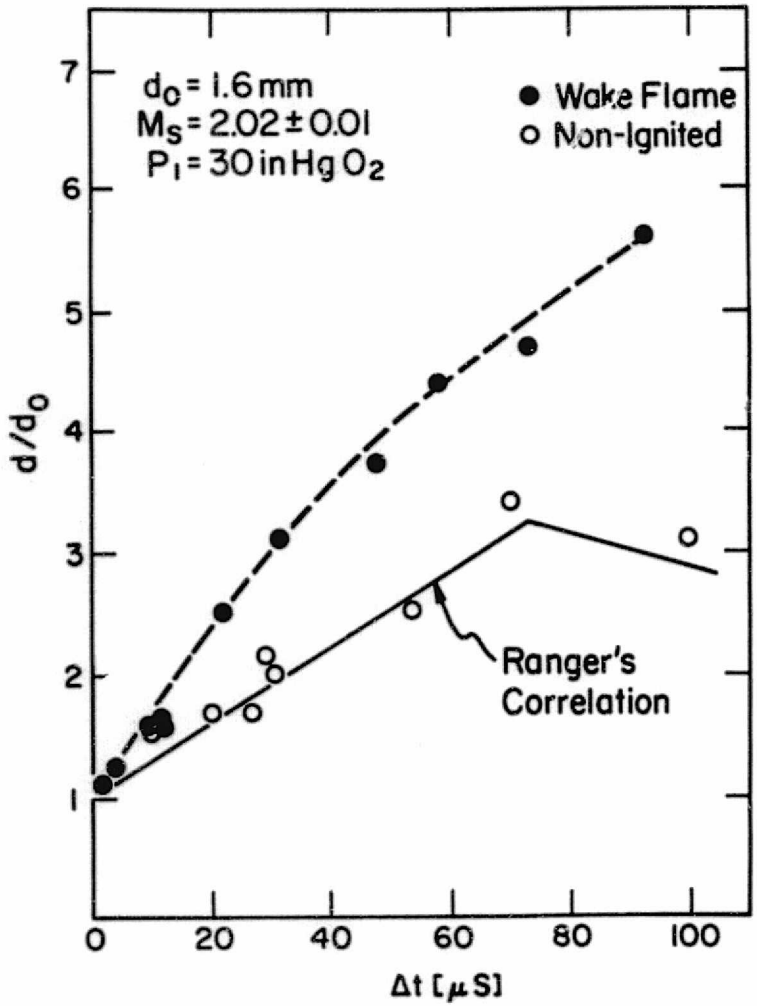

Figure 7. Drop Deformation, Wake Flame Conditions.

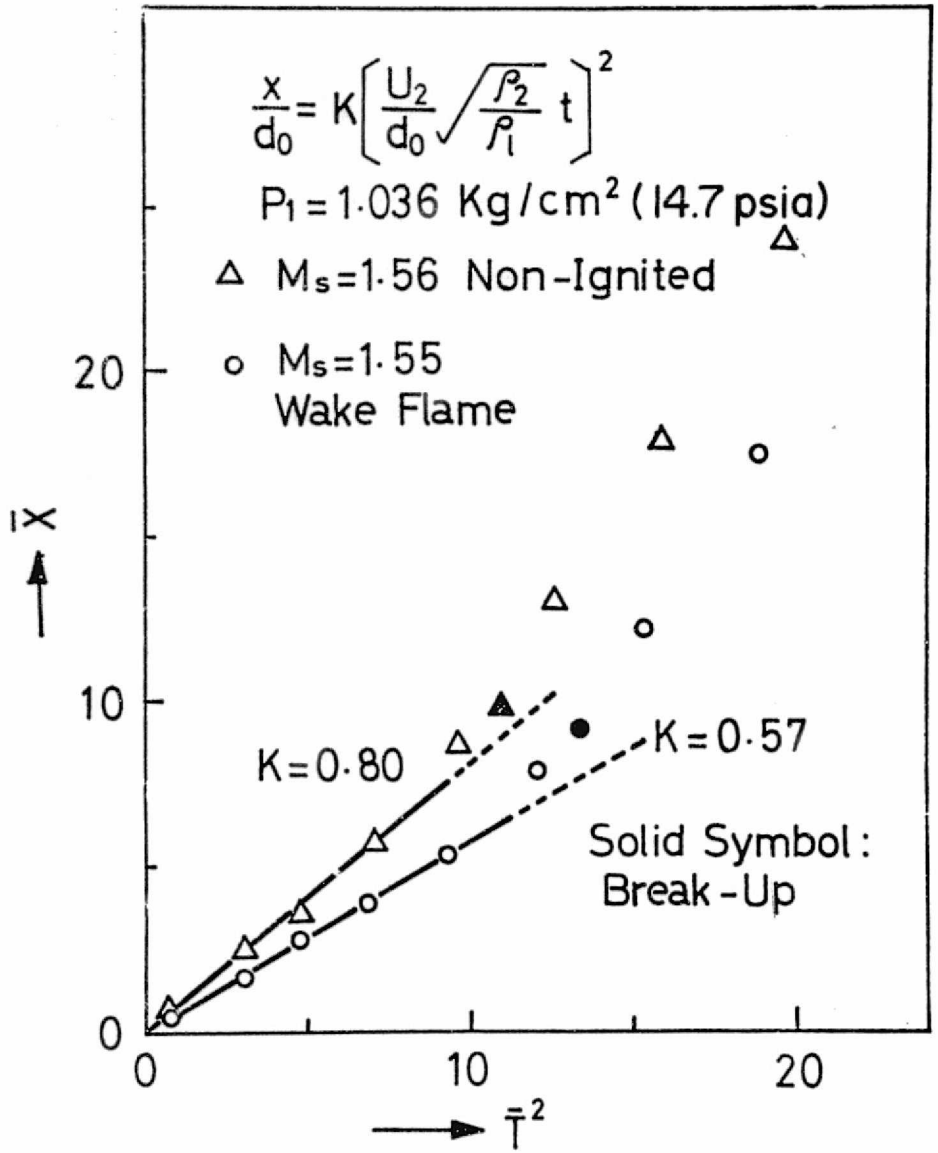

Figure 8. Drop Displacement Parallel to the Direction of Flow.

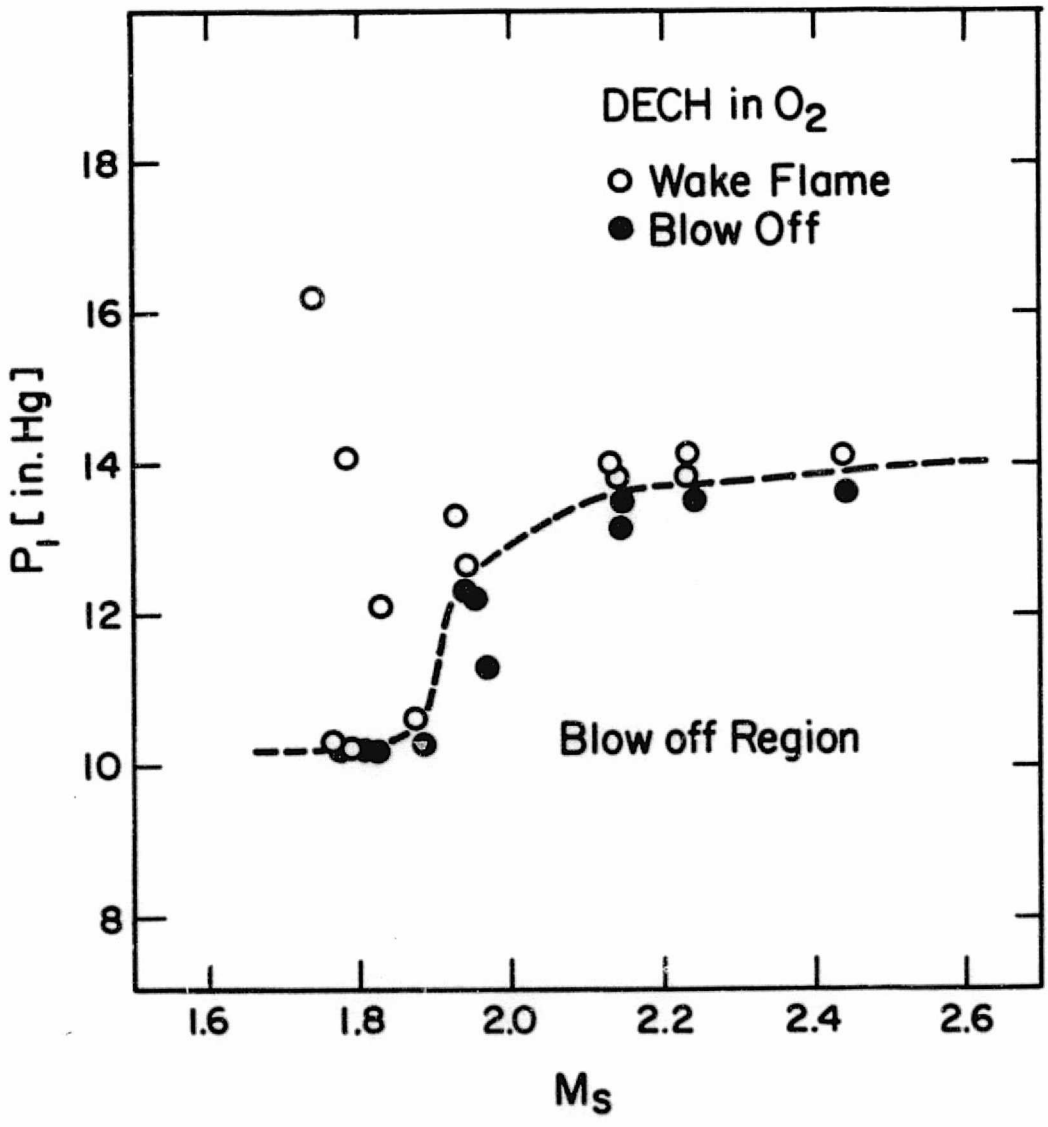

Figure 9. Limiting Initial Pressure of Pure Oxygen for Blow Off.

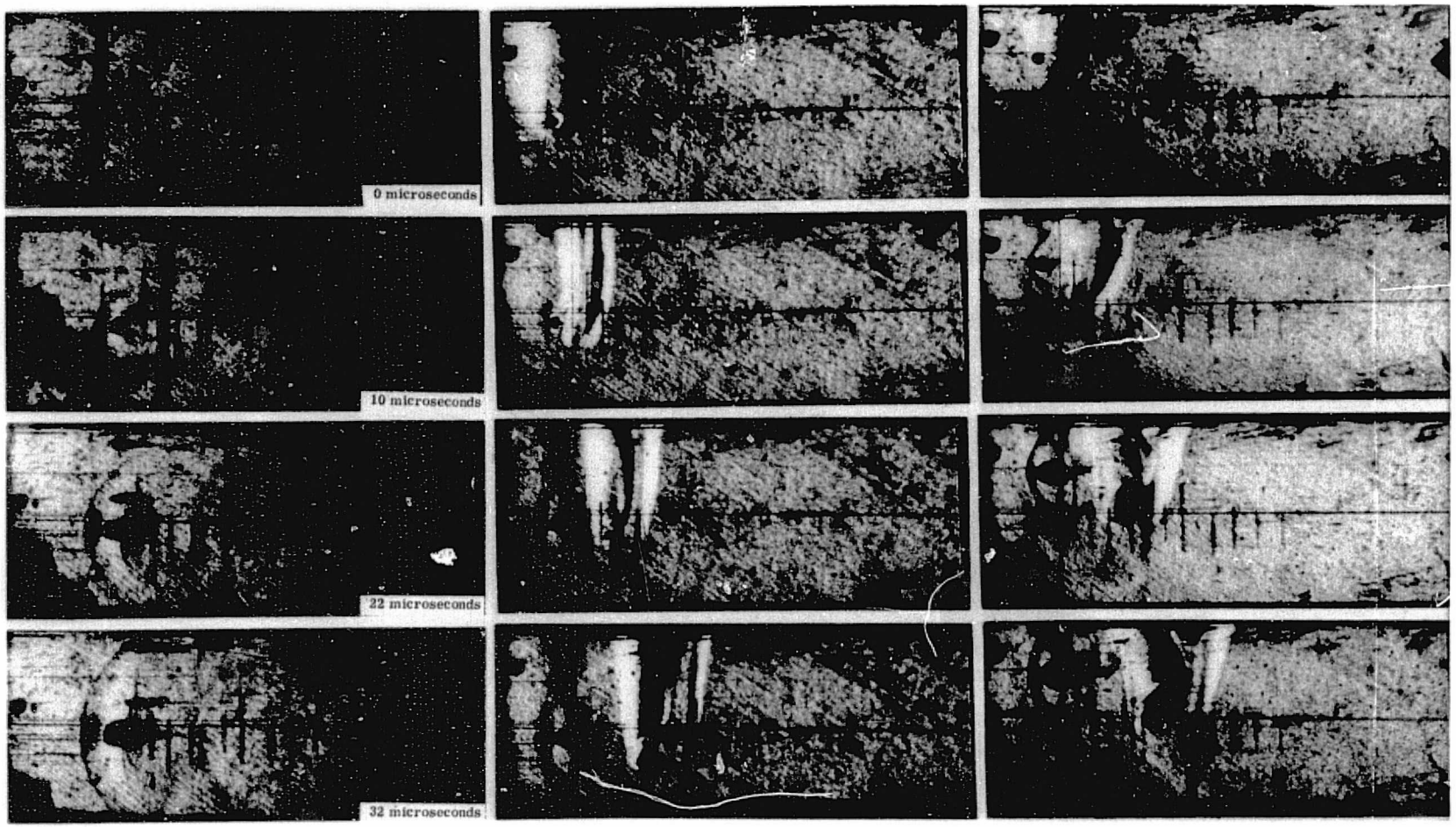

Figure 10. Comparison of Initially Non-Ignited and Ignited Drops at $M_s = 2.05$, $P_1 = 29.1$ in. Hg in Nitrogen, Air and Oxygen.

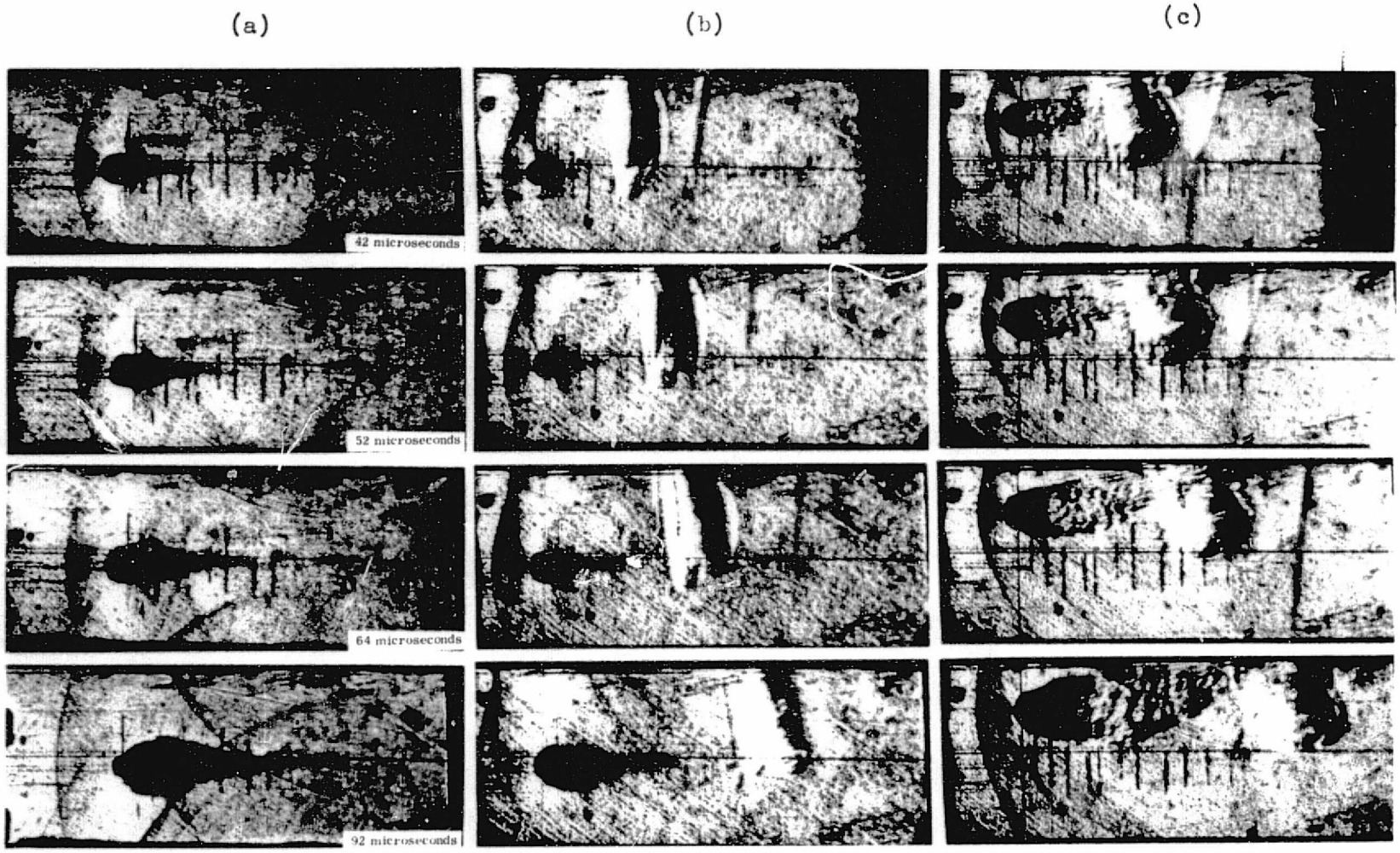

Figure 10. Concluded.

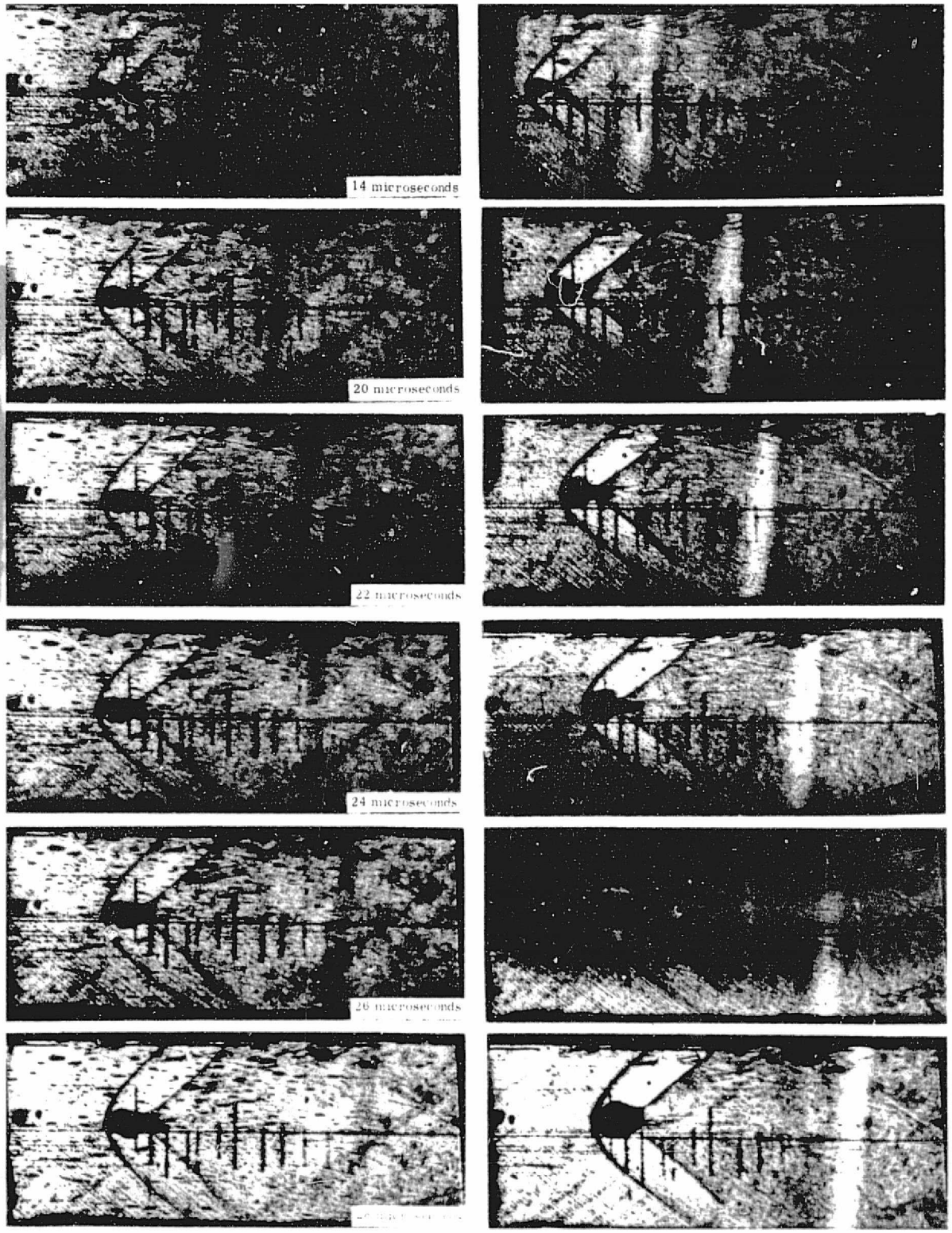

Figure 11. Strong Shock Wave over Non-Ignited Drops in N_2 and O_2; $M_s = 3.5$, $P_1 = 29.1$ in. Hg.

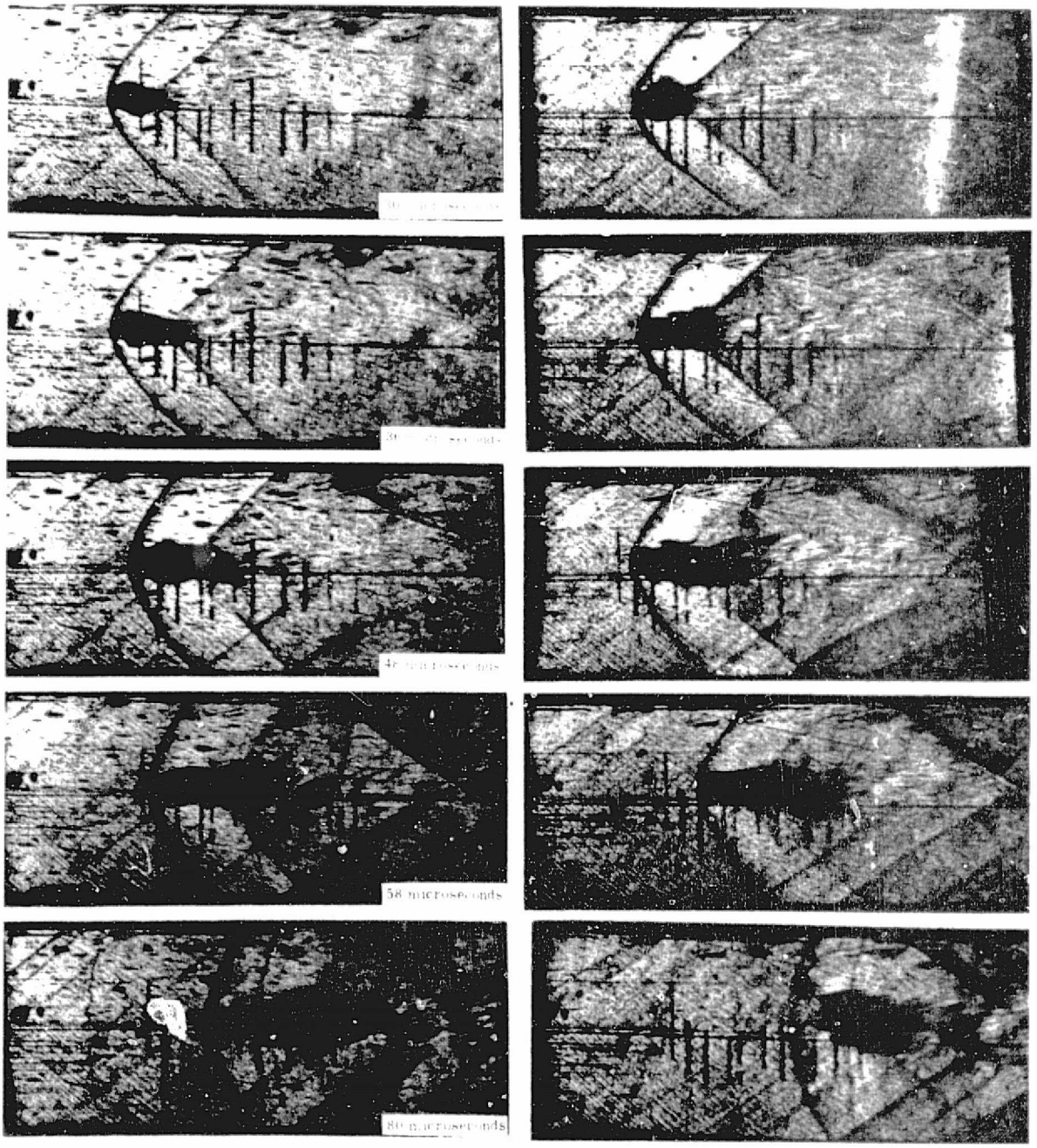

(d) (e)

Figure 11. Concluded.

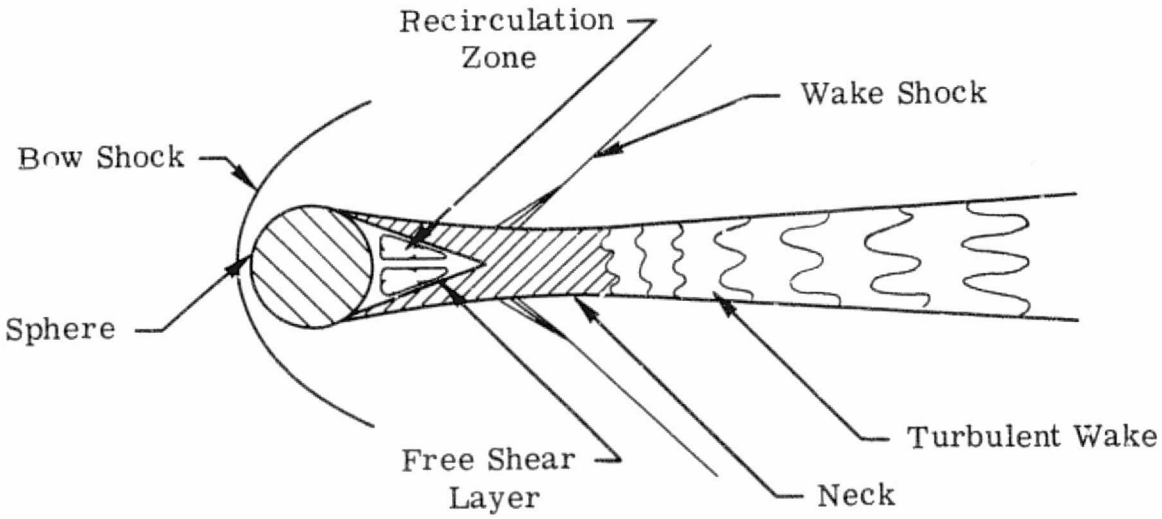

Figure 12. Supersonic Flow over a Sphere.

Figure 13. Shock Wave over a Water Drop, d = 750 μm, M_s = 2.7, t = 2.6 μs.

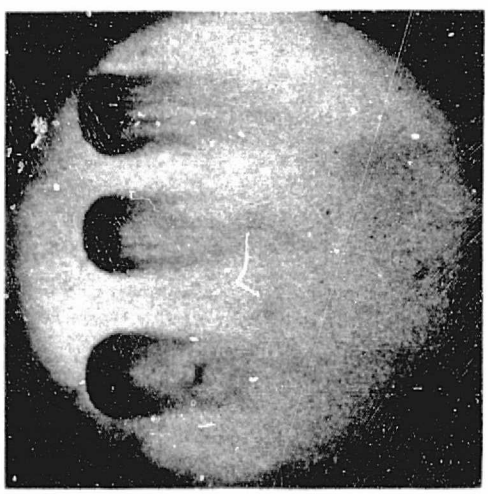

Figure 14. Shock Wave over a Water Drop, d = 750 μm, M_s = 2.0, t = 15.8 μs.

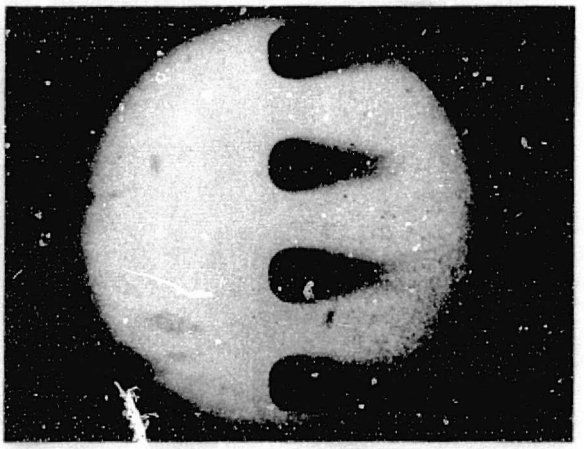

(a)

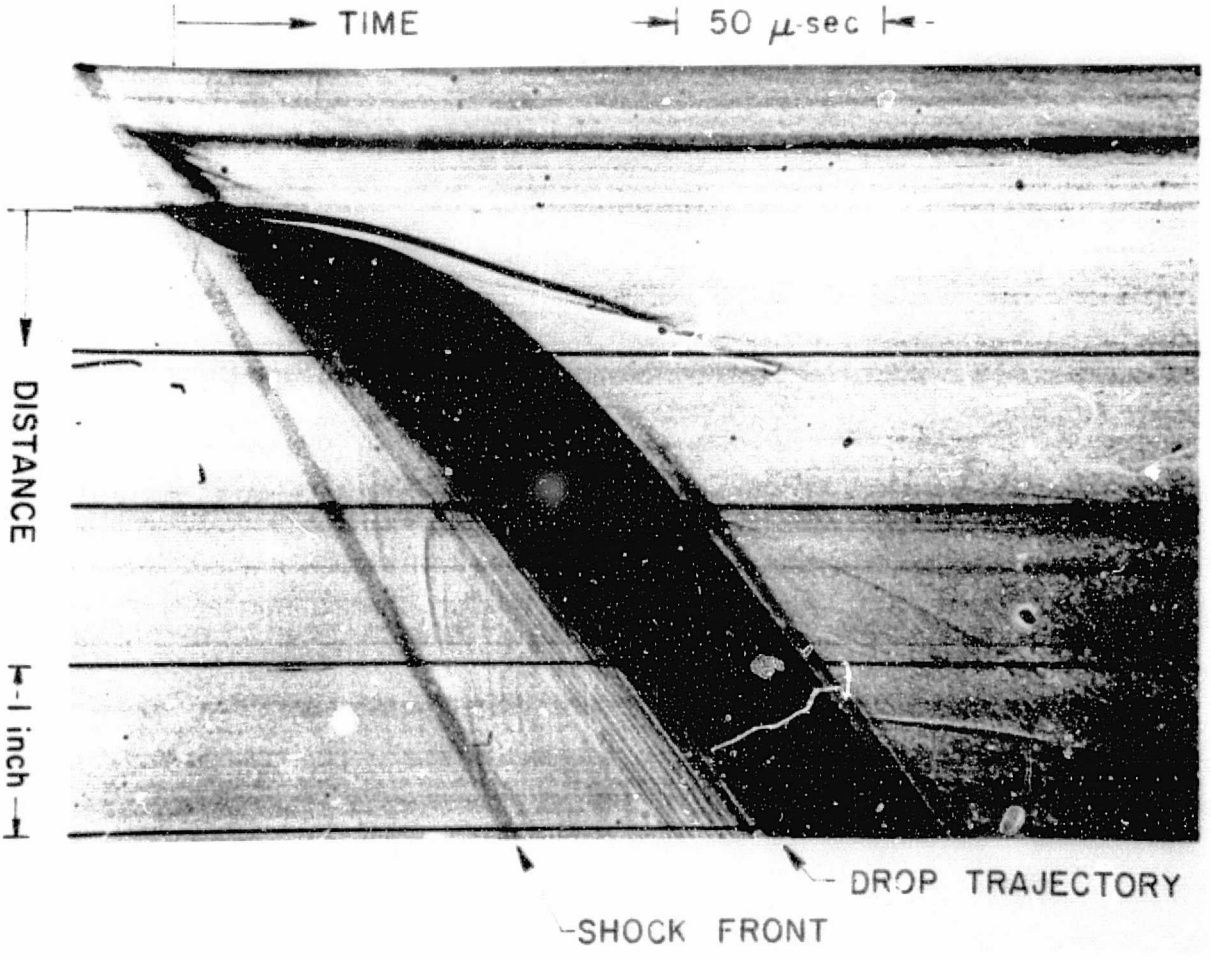

(b)

Figure 15. Shock Wave over a Water Drop,
(a) $d = 750\ \mu m$, $M_S = 2.7$, $t = 4.4\ \mu s$
(b) $d = 1400\ \mu m$, $M_S = 3.34$.

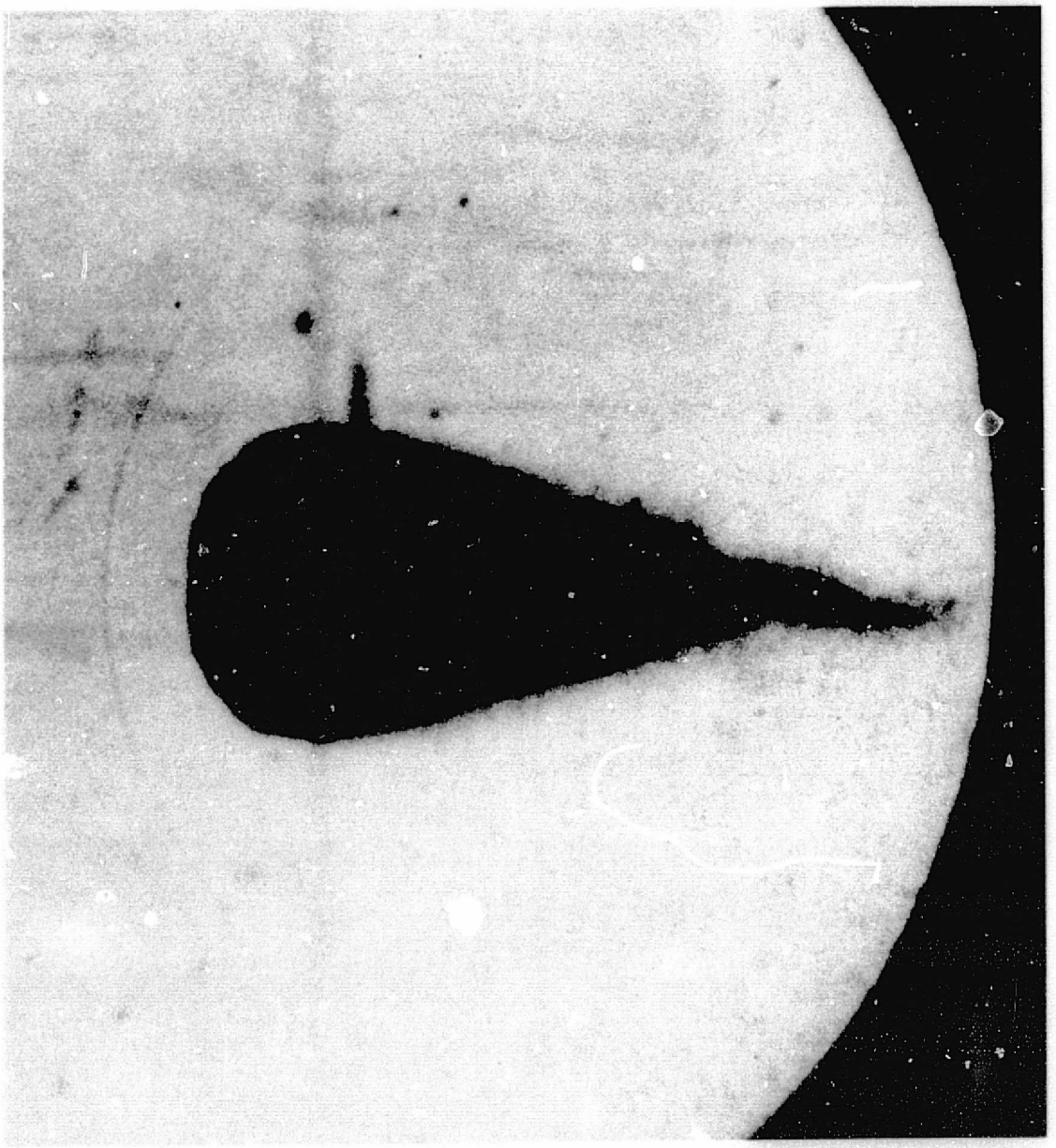

Figure 16. Shock Wave over a Water Drop, $d = 2700\ \mu m$, $M_s = 3.5$, $t = 14\ \mu s$.

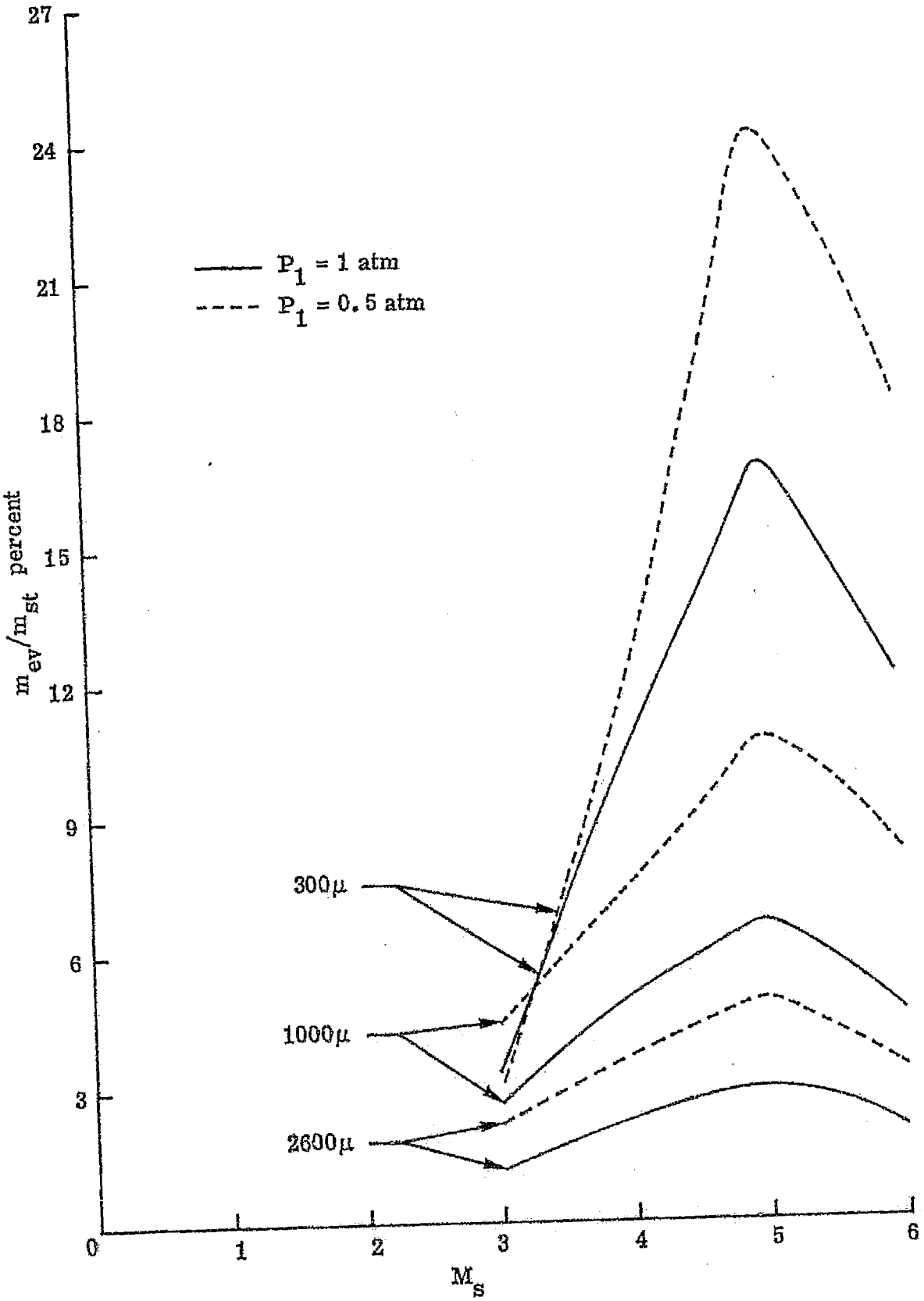

Figure 17. m_{ev}/m_{st} vs M_s.

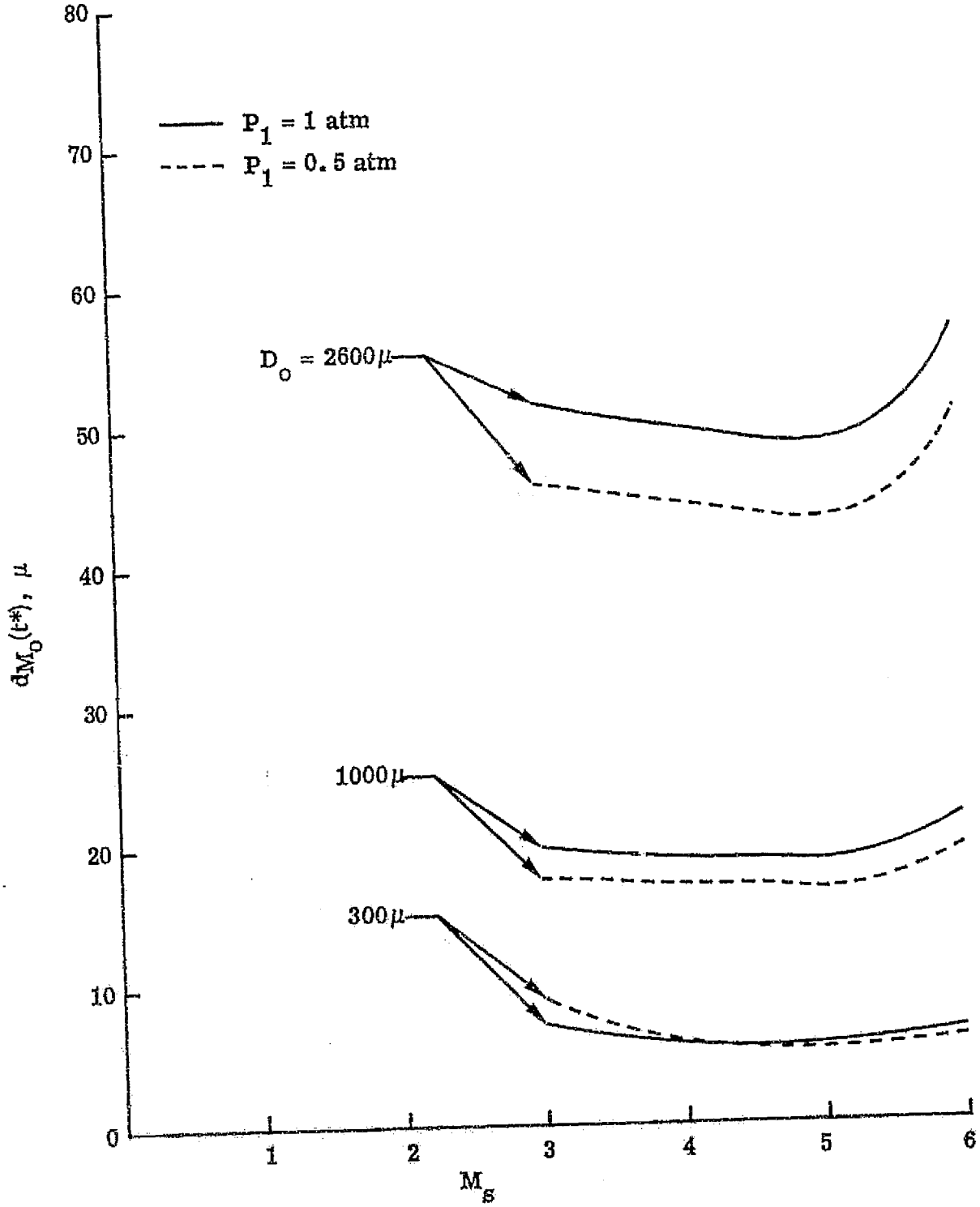

Figure 18. d_{M_o} vs M_s.

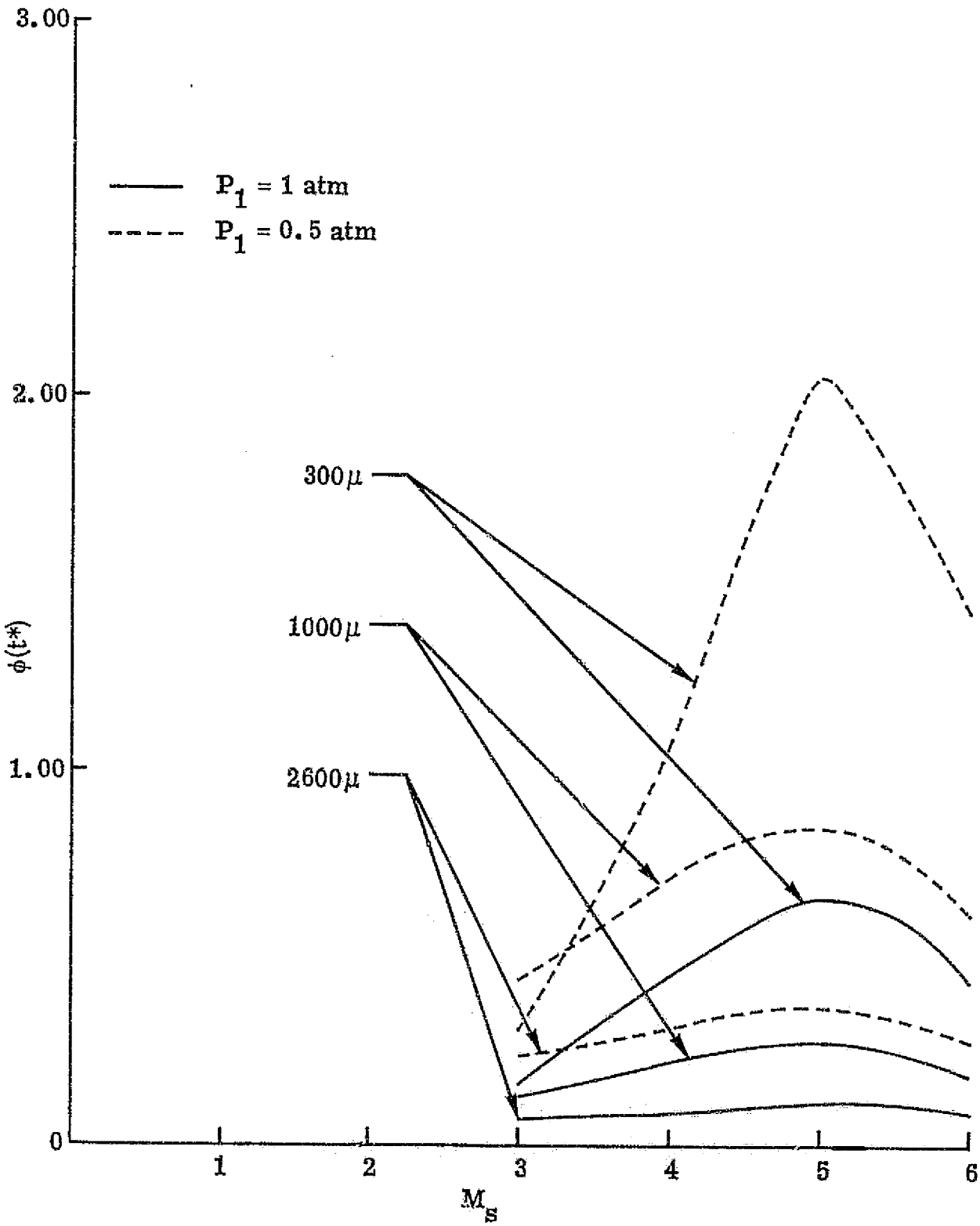

Figure 19. $\phi(t^*)$ vs M_s.

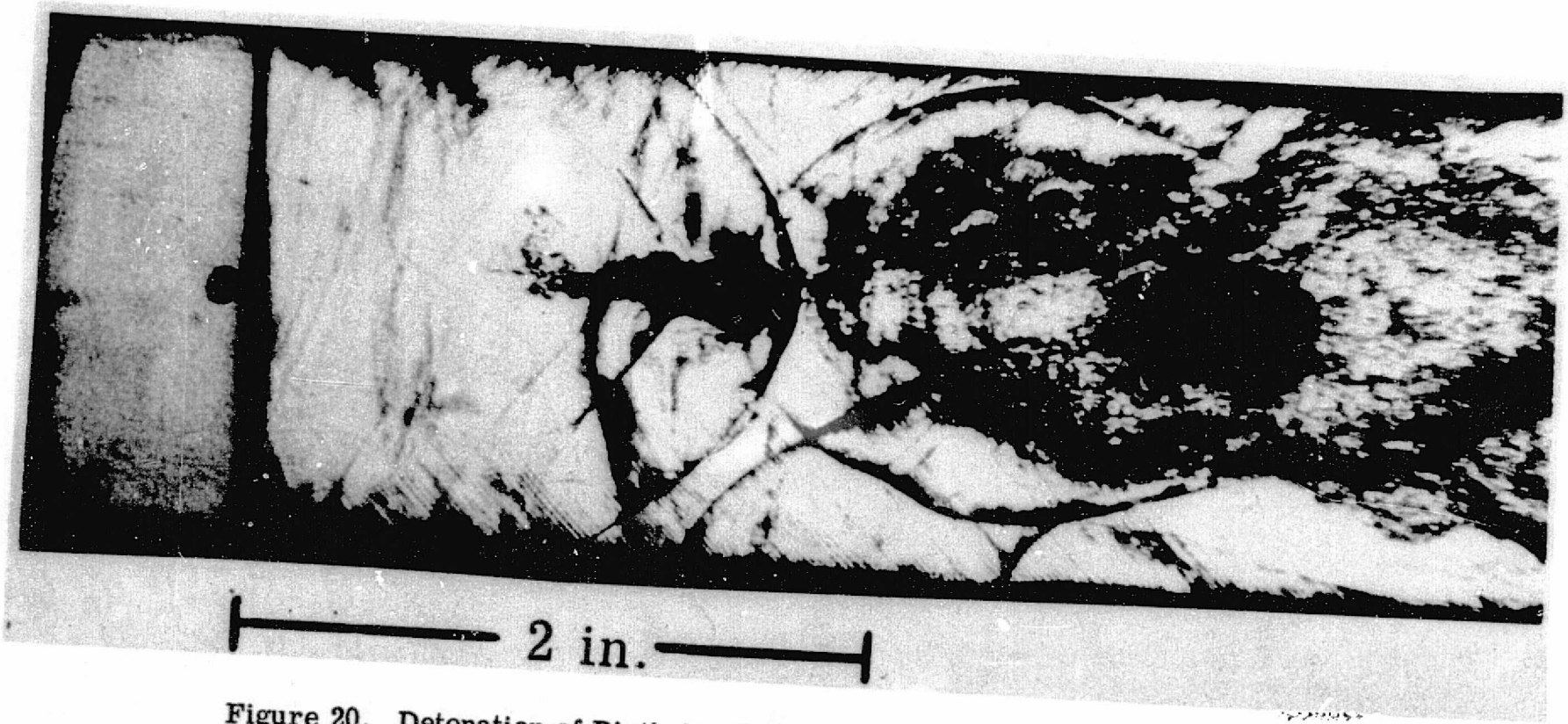

Figure 20. Detonation of Diethylcyclohexane Drops in Oxygen, d = 2600 μm.

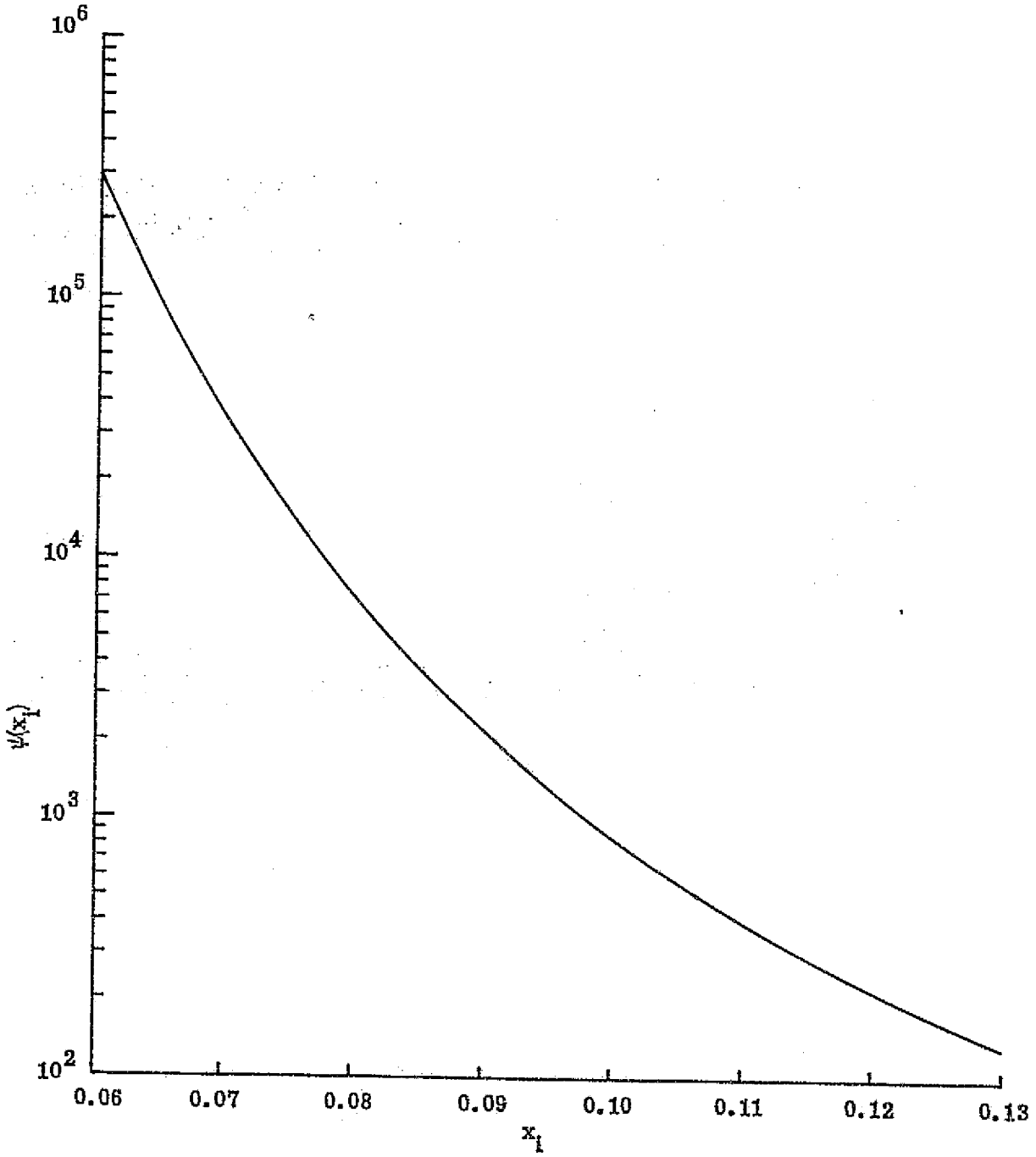

Figure 21. $\psi(x_i)$ vs x_i.

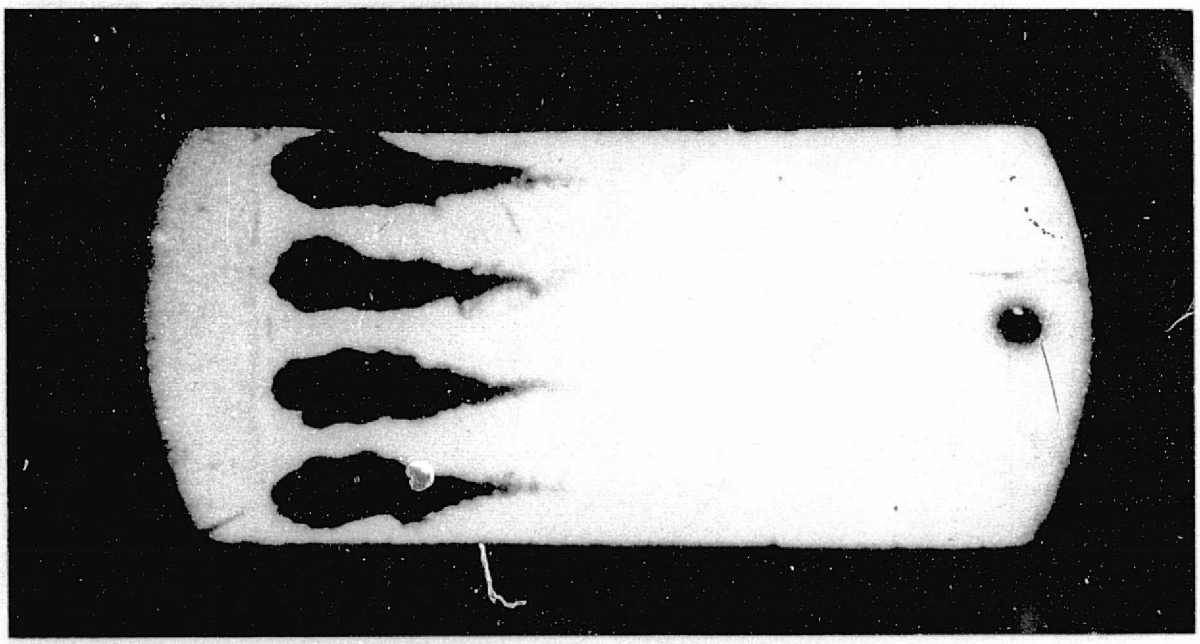

Figure 22. Shock Wave over Water Drops, $M_s = 3.25$, $t = 38.8\ \mu s$.

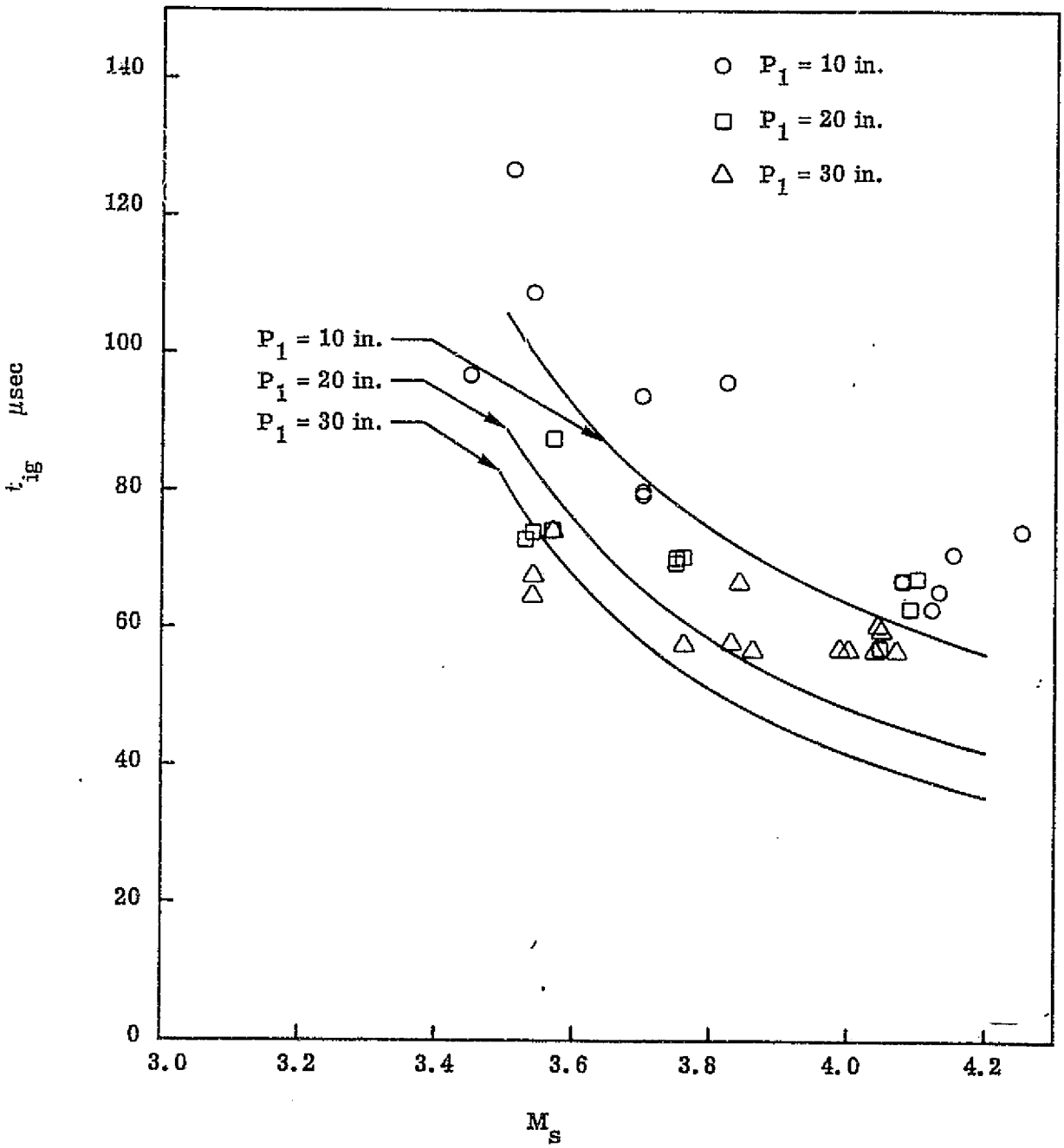

Figure 23. Ignition Time vs M_s, d = 2130 μm.

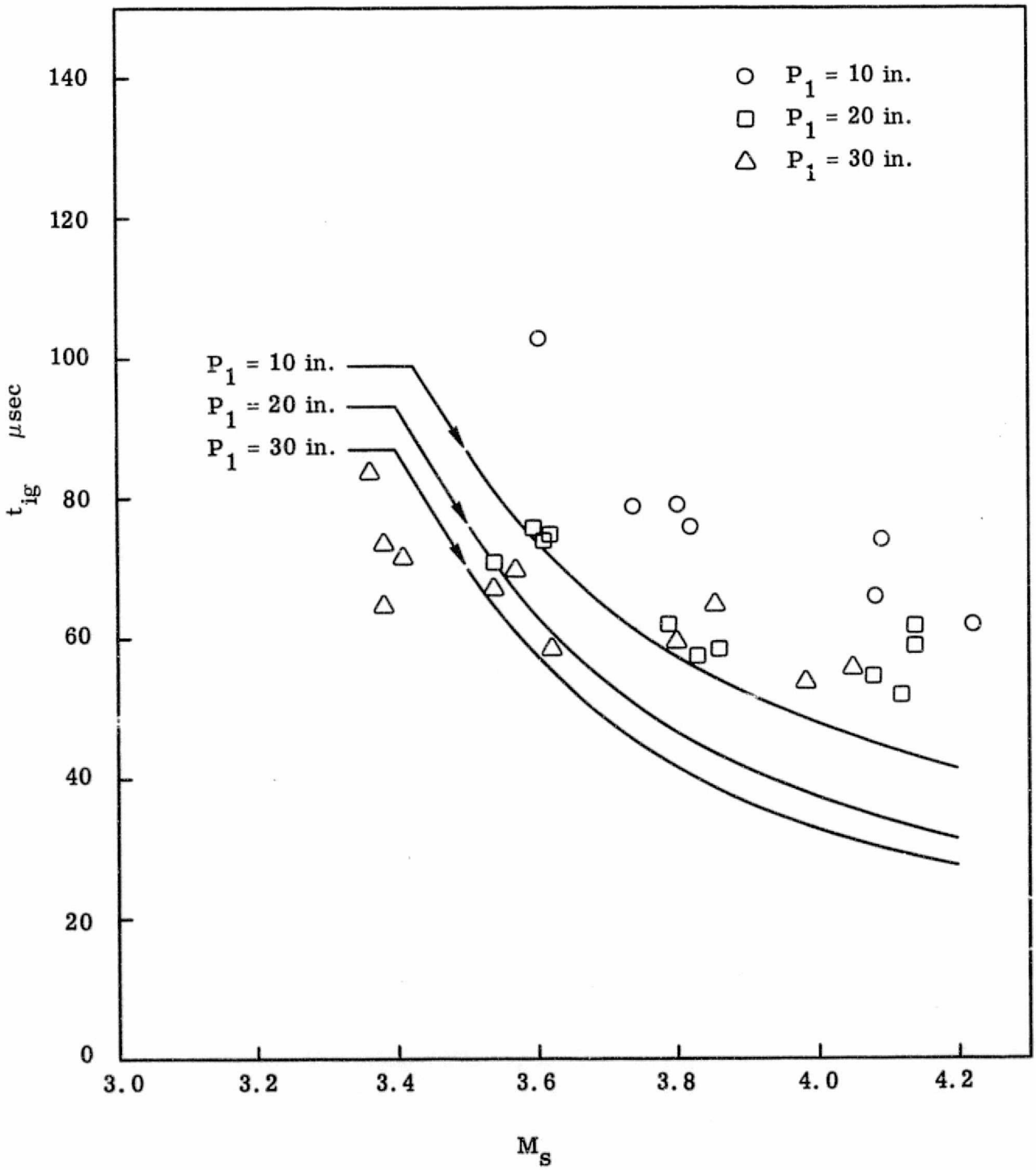

Figure 24. Ignition Time vs M_s, d = 1520 μm.

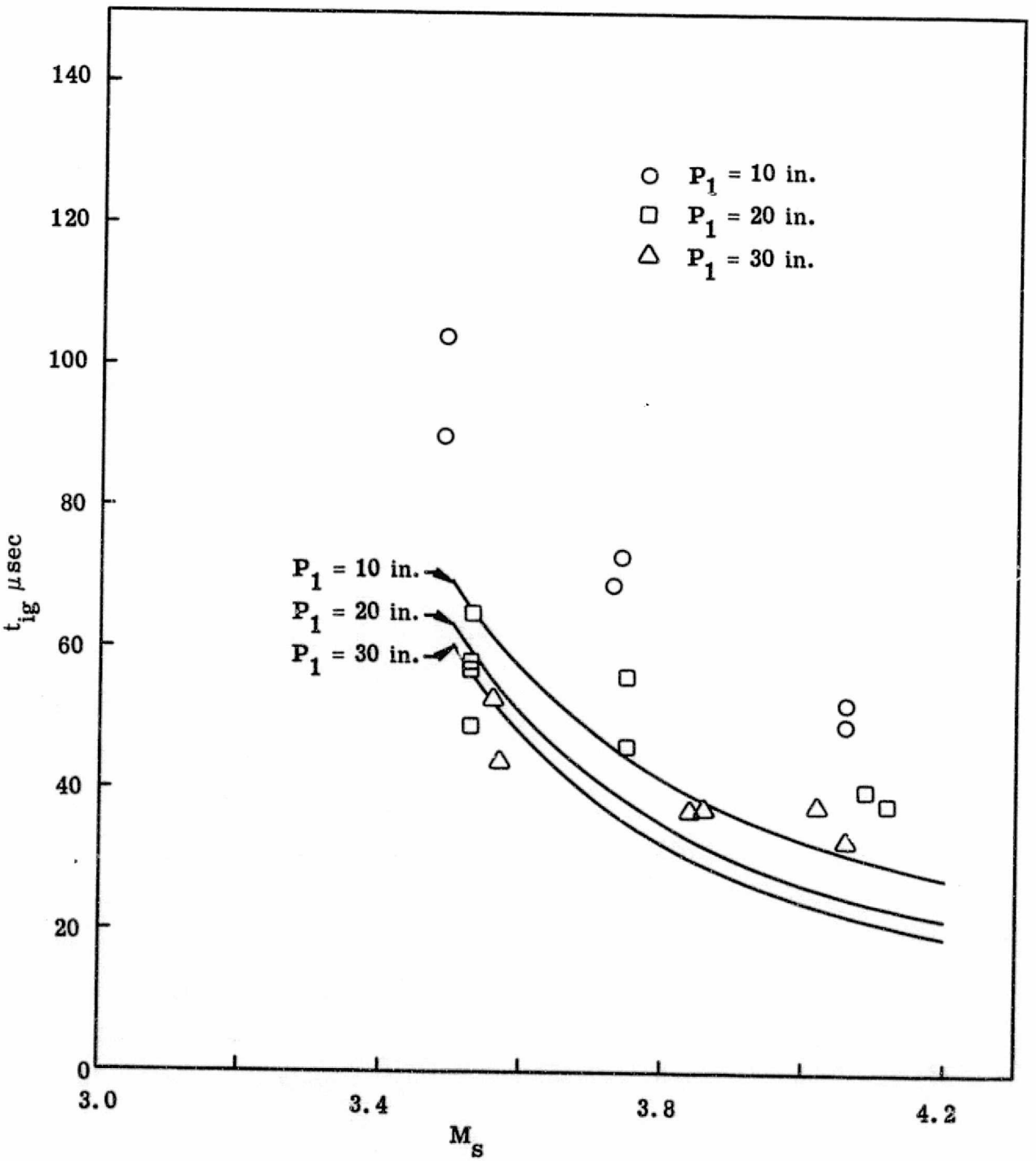

Figure 25. Ignition Time vs M_s, d = 932 μm.

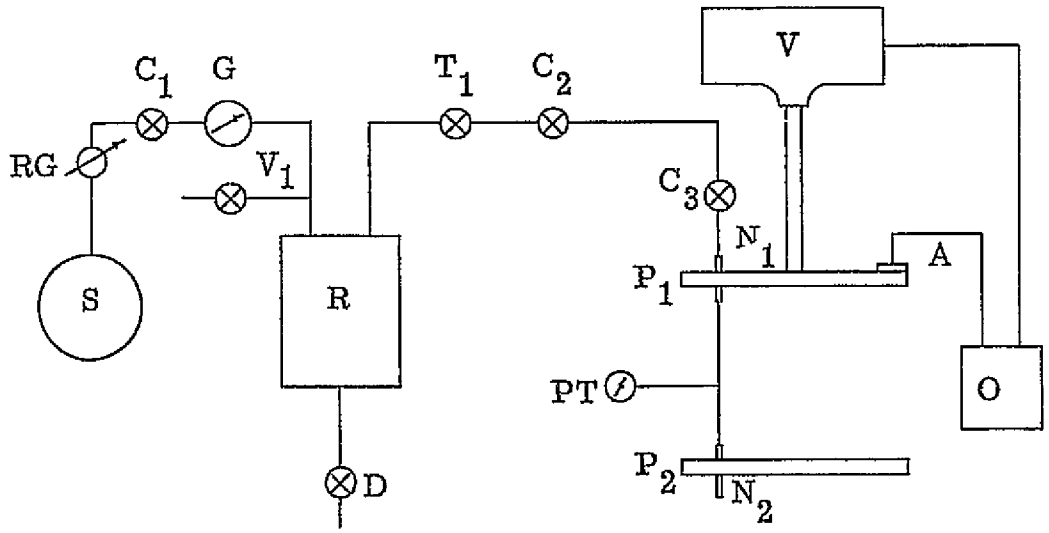

Figure A-1. Schematic of the Apparatus

A	Accelerometer	C_1	Supply Pressure Valve
C_2	Coarse Metering Valve	C_3	Fine Metering Vlave
D	Drain Valve	N_1	Vibrated Tube
N_2	Stationary Capillary	O	Dual Beam Oscilloscope
P_1	Vibrated Platform	P_2	Stationary Platform
PT	Pressure Transducer	R	Test Liquid Reservoir
RG	Pressure Regulator	S	Nitrogen Supply Bottle
T_1	Toggle Valve	V_1	Supply Pressure Vent
		V	Shaker

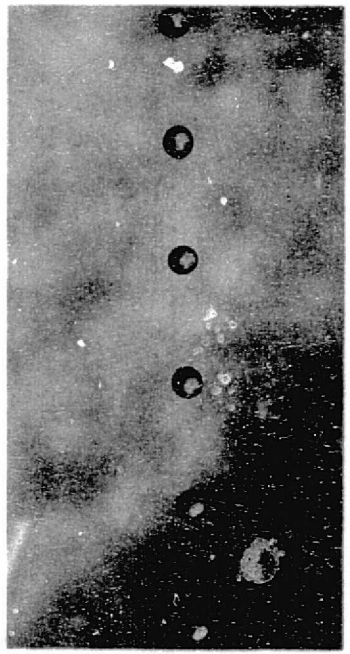

Figure A-2. Drop Formation with Correct Power Setting.

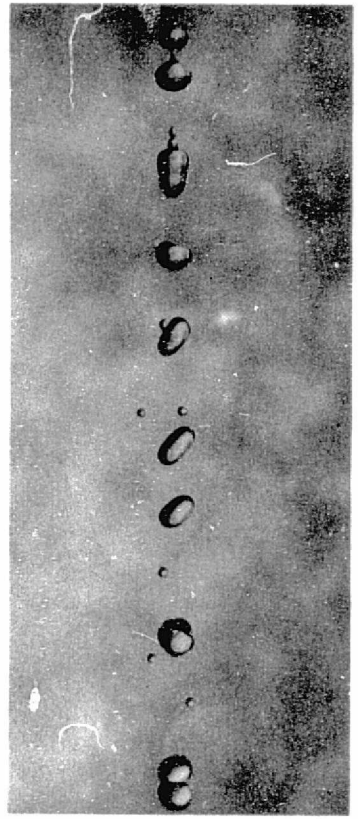

Figure A-3. Drop Formation with Insufficient Power.

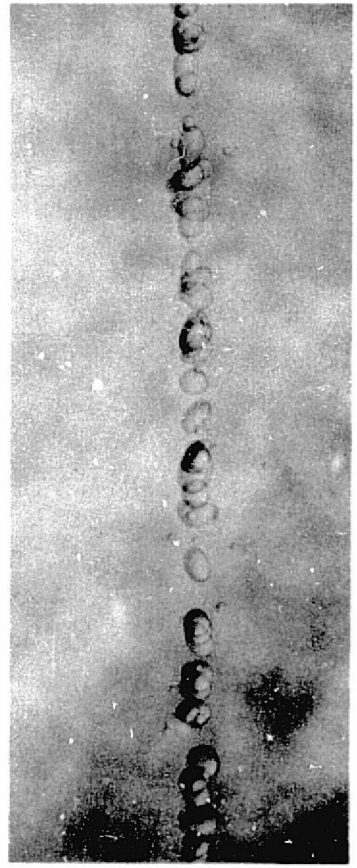

Figure A-4. Natural Drop Formation—No Power.

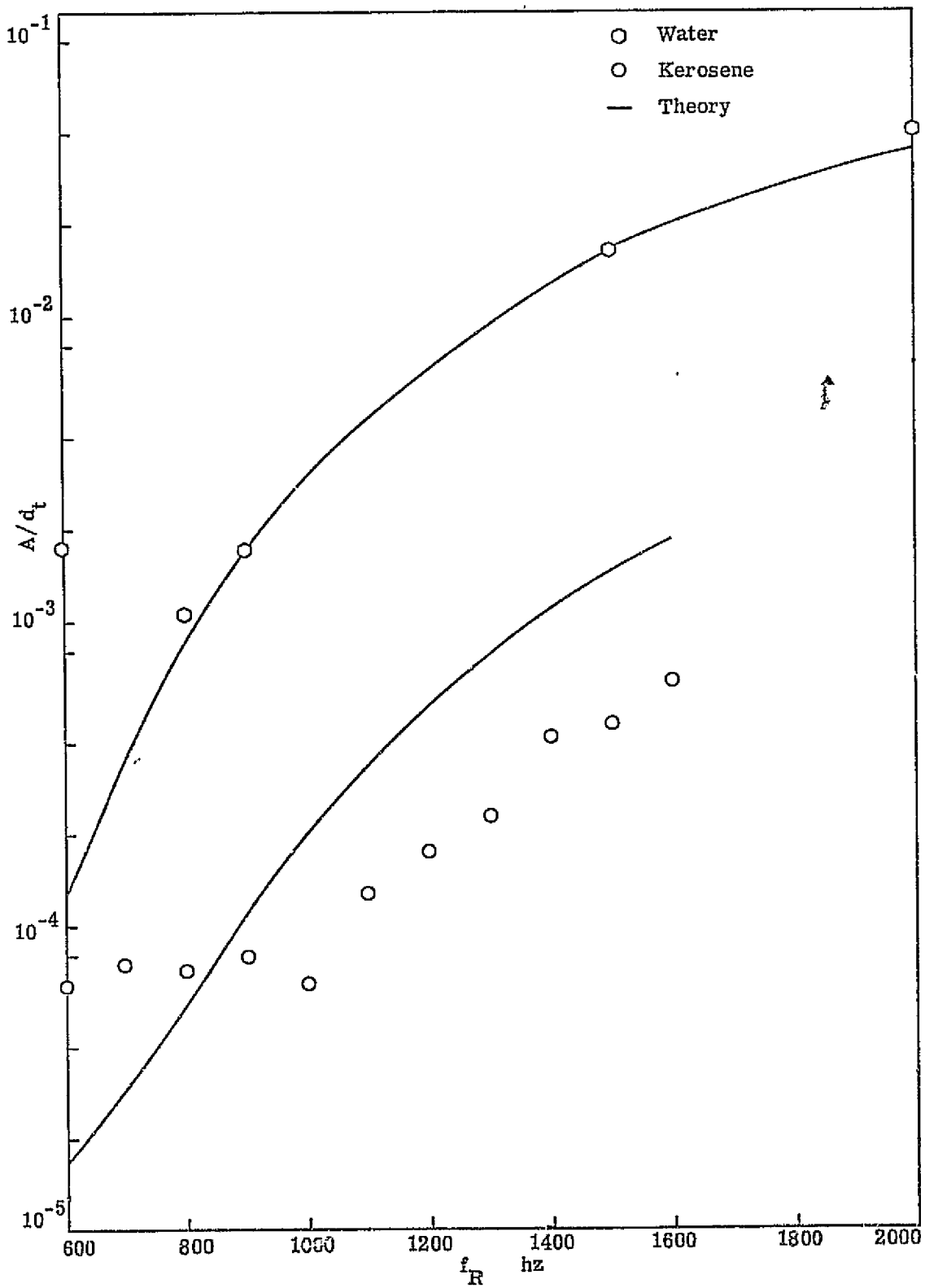

Figure A-5. Comparison of Experimental and Theoretical Results -- Water, Kerosene.

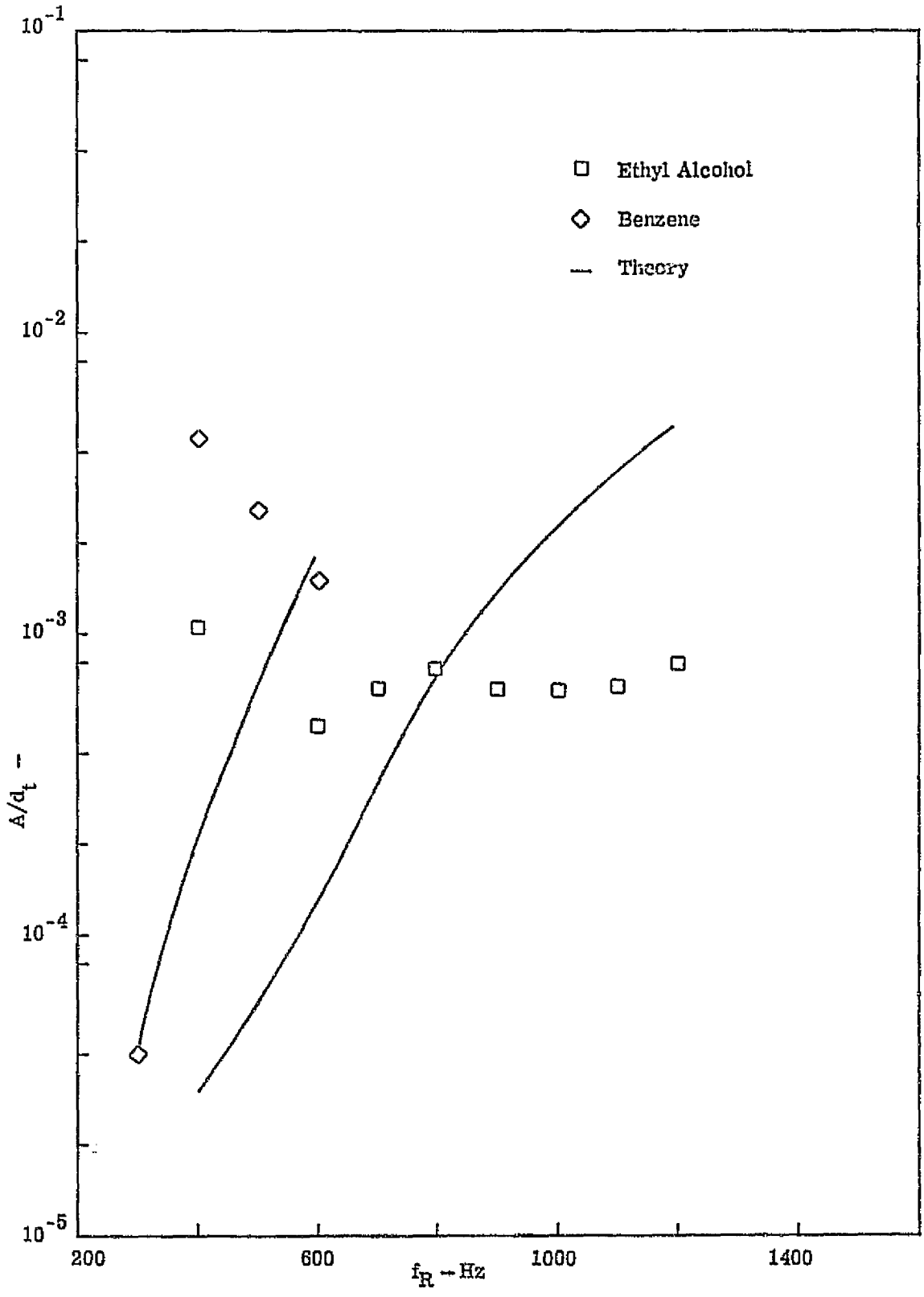

Figure A-6. Comparison of Experimental and Theoretical Results— Ethyl Alcohol, Benzene.